Scaling patterns of cerebellar petrosal lobules in Euarchontoglires

Lang Madlen Maryanna (Orcid ID: 0000-0003-2604-4733)
Bertrand Ornella C. (Orcid ID: 0000-0003-3461-3908)

Scaling Patterns of Cerebellar Petrosal Lobules in Euarchontoglires: Impacts of Ecology and Phylogeny

MADLEN M. LANG[1*], ORNELLA C. BERTRAND[2], GABRIELA SAN MARTIN FLORES[3], CHRIS J. LAW[4,5,6], JADE ABDUL-SATER[1], SHAYDA SPAKOWSKI[1], MARY T. SILCOX[1].

[1]Department of Anthropology, University of Toronto Scarborough, Toronto, ON M1C 1A4, Canada
[2]School of GeoSciences, University of Edinburgh, Grant Institute, Edinburgh, EH8 9XP, Scotland, UK
[3]Flinders University, College of Science and Engineering, Bedford Park, SA 5042, Australia
[4]Richard Gilder Graduate School, Department of Mammalogy, and Division of Paleontology, American Museum of Natural History, 200 Central Park West, New York, NY 10024;
[5]Department of Biology, University of Washington, Seattle, WA, 98105
[6]The University of Texas at Austin, Austin, TX, 78712

*e-mail: madlen.lang@mail.utoronto.ca

This article has been accepted for publication and undergone full peer review but has not been through the copyediting, typesetting, pagination and proofreading process which may lead to differences between this version and the Version of Record. Please cite this article as doi: 10.1002/ar.24929

ABSTRACT

The petrosal lobules (in whole or part homologous with the paraflocculi) of the cerebellum regulate functions associated with vision including smooth pursuit and velocity control of eye movements, suggesting a possible relationship between the petrosal lobules and behavioral adaptation. Previous studies have produced diverging conclusions regarding the lobules' ecological signal. The current study examines lobule scaling within an ecologically diverse but phylogenetically constrained sample of extant mammals to determine if ecology influences relative petrosal lobule size. Using the endocasts of 140 Euarchontoglires (Primates, Scandentia, Dermoptera, Lagomorpha, Rodentia), petrosal lobule size was evaluated relative to endocranium and body size, accounting for phylogenetic relationships and ecology (locomotor behavior, diet, activity pattern). Results show a strong positive relationship between lobule size and both endocranial volume and body mass. Phylogeny is a major factor in the scaling of the petrosal lobules, with significant differences in relative size identified between orders and suborders. Concerning ecology, fossorial taxa were found to have significantly smaller petrosal lobules relative to body mass compared to other locomotor groups across Euarchontoglires. The small lobules possessed by this group may reflect an adaptation related to reduced visual reliance. In contrast to previous research, no relationship was identified between relative lobule size and any other ecological variables. While variation in relative lobule size may be adaptively significant in some groups (i.e. fossorial species), it is critical to study the evolution of petrosal lobule size within a narrow phylogenetic scope, with inclusion of fossil material to inform our understanding of evolutionary trajectories.

Key words: Endocast; Petrosal Lobule; Neuroanatomy; Paraflocculi; Euarchontoglires; Ecology

1 |INTRODUCTION

Analyses of the scaling patterns of the mammalian brain and its components provide valuable information about how the brain responds to selective pressures and can help identify broader evolutionary trends. To this end, numerous studies have drawn connections between ecological specialization and variation in the size and morphology of the mammalian brain and its particular structures (e.g., Barton and Harvey, 2000; de Winter and Oxnard, 2001; DeCasien and Higham, 2019). These studies generally operate on the premise that an adaptation requiring an increase in the information sent to certain neural tissues will result in an increase in the relative size of those tissues (i.e., Jerison's [1973, 1979] principle of proper mass), and therefore variation in the relative sizes of functionally significant brain tissues reflect adaptive specialization (Barton and Harvey, 2000).

The evolutionary relevance of interspecific variation in the brain and its parts in relation to sensory and cognitive adaptations has been extensively investigated in primates (DeCasien and Higham, 2019). Variation in the size of neocortex, the olfactory bulbs, and in functionally significant cortical regions have been attributed to ecological behaviors associated with vision and activity pattern (Barton et al., 1995; Barton, 1998; Kirk, 2006; Powell et al., 2017), diet and foraging strategy (Clutton-Brock and Harvery, 1980; Harvey et al., 1980; Powell et al., 2017; DeCasien et al., 2017; DeCasien and Higham, 2019), and sociality (Dunbar, 1992, 1995; Sawaguchi and Kudo, 1999; Kudo and Dunbar, 2001; Barton, 2006; Dunbar and Shultz, 2007). Similar ecology-related scaling patterns have also been identified in rodents (e.g., Lemen, 1980; Mace et al., 1981; Roth and Thorington, 1982; Meier, 1983; Pilleri et al., 1984; Bernard and Nurton, 1993; Krubitzer et al., 2011; Bertrand et al., 2017; 2018; 2019b; 2021) and in other small mammals (Bhatnagar and Kallen, 1974; Eisenberg and Wison, 1978, 1981; Harvey et al., 1980;

Mace et al., 1981; Gittleman, 1986, 1991; Barton et al., 1995; de Winter and Oxnard, 2001). These studies indicate that species belonging to independent lineages can exhibit neurologic convergences in functionally and ecologically important brain structures, causing brain architecture to diverge from those of phylogenetically closer species (de Winter and Oxnard, 2001).

The widespread availability of high-resolution X-ray Computed Tomography (CT) data has led to the proliferation of studies evaluating variation in the endocast and endocranium of extinct and extant groups (Balanoff and Bever, 2020). Of these studies however, comparatively few have focused on the evolution of the mammalian cerebellum and its components specifically, within the context of variation as a function of ecological and behavioral factors (Ridgway and Hanson, 2014; Barks et al., 2015; Ferreira-Cardoso et al., 2017). One component of the cerebellum, the petrosal lobules, are of particular interest. As part of the vestibulocerebellum (or archicerebellum), the petrosal lobules are among the evolutionarily oldest anatomical components of the cerebellum (Kheradmand and Zee, 2011). The vestibulocerebellum is comprised of the nodulus, ventral uvula, and floccular-paraflocculare complex (Kheradmand and Zee, 2011). Together, these brain structures play a major role in the stabilization of eye movements and in the vestibuloocular reflex (VOR) (Rambold et al., 2002; Hiramatsu et al., 2008; Kheradmand and Zee, 2011). Within the vestibulocerebellum, the petrosal lobules are part of the floccular-paraflocculare complex, sometimes referred to as the "floccular lobe" (Krauzlis and Lisberger, 1994; Fukushima et al., 1999), "floccular complex" (Rambold et al., 2002), or ''floccular region'' (Belton and McCrea, 2000a,b). The floccular-paraflocculare complex includes the flocculi, paraflocculi, and the petrosal lobules (as a component of the paraflocculi). These tissues receive visual and vestibular information from the

visual cortex and the semicircular canals, and output to the ocular muscles to regulate eye movements (Burne and Woodward, 1983; Voogd and Barmack, 2006; Hiramatsu et al., 2008). Specifically, the floccular-parafloccular complex stabilizes visual images on the retina by generating compensatory eye movements (Rambold et al., 2002), regulates smooth pursuit eye movements to prevent retinal image blur of a moving object (Zee et al., 1981; Shojaku et al., 1990; Nagao, 1992; Rambold et al., 2002; Ilg and Their, 2008), and velocity control of eye movements (Hiramatsu et al., 2008). The petrosal lobules themselves extend laterally from the cerebellum to fill a distinct cavity in the cranium called the subarcuate fossa in many vertebrate groups including mammals (Gannon et al., 1988), birds (Walsh et al., 2013), and pterosaurs (Witmer et al., 2003) (Figure 1). The fossa is formed by the petrosal bone and extends through the arch of the anterior semicircular canal (Gannon et al., 1988; Figure 2).

The homology of the cerebellar structures that are housed in the subarcuate fossa can vary between orders, which has implications for their nomenclature and how we understand their functions between taxa. In Glires (Tan et al., 1995; Panezai et al., 2019) and Scandentia (Ni et al., 2018) the lobules are formed by the paraflocculi, which are divided into the ventral and dorsal paraflocculus (Tan et al., 1995). In contrast, the petrosal lobules of primates are formed by only a portion of the paraflocculi (Voogd and Barmack, 2006). While the dorsal and the ventral paraflocculus are functionally linked to the petrosal lobules (Voogd et al., 2012), they sit within the endocranial cavity adjacent to the flocculus and subarcuate fossa (Xiong et al., 2010). Previous analysis examining the scaling of the subarcuate fossa and the petrosal lobules/paraflocculus of mammals, including primates, rodents, and lagomorphs, found a strong correlation between the size of the fossa and the tissues which sit inside it (Gannon et al., 1988). Significantly, this means it is possible to obtain an estimate of the size of these lobules using the

subarcuate fossa. As a result, we use the term 'petrosal lobule' to refer to the tissue occupying the subarcuate fossa instead of 'paraflocculus' for all taxa in this analysis for two reasons: 1) this sample includes primates and therefore the paraflocculi is not being measured *per se* across all taxa, and 2) as we are using endocasts and not neural tissue, any measurements obtained represent the potential maximum volume of the tissue occupying the subarcuate fossa of the petrosal bone and consequently, the term "petrosal lobule" is more accurate in describing what can be measured.

As the petrosal lobules are protected inside the subarcuate fossa, they are difficult to study using microelectrode techniques and therefore their specific function as part of the floccular-paraflocculus complex is difficult to assess (Hiramatsu et al., 2008). Nevertheless, there is strong evidence that the petrosal lobules play a key role in smooth pursuit and velocity control of eye movements (Hiramatsu et al., 2008). Within primates, the petrosal lobules receive projections from the dorsolateral pontine nucleus (Glickstein et al., 1994; Nagao et al., 1997; Xiong and Nagao, 2002; Xiong et al., 2010), which represents a major relay area for smooth pursuit eye movements to the cerebellum (May et al., 1988). Further connections to the lobules have been identified in the medial temporal/medial superior temporal extrastriate visual areas of the parietal cortex (Glickstien et al., 1994), also known as important sites for smooth pursuit eye movements (Newsome et al., 1988). The lobules also project to pre-oculomotor structures via the lateral interstitial nuclei (Xiong and Nagao, 2002). Significantly, lesioning of the lobules in macaques reduced the velocity of smooth pursuit eye movements (Hiramatsu et al., 2008). There have been no systematic studies of the functional role of the rodent paraflocculi (= petrosal lobules). However, the neural connections of the ventral and dorsal paraflocculi of the rat are consistent with those of the macaque ventral and dorsal paraflocculi (Osanai et al., 1999) which

play a role in smooth pursuit eye movements as well as VOR adaptations (Rambold et al., 2002). Like the primate petrosal lobules, the paraflocculi of rodents appear to be a major receiving area of the cerebellum for information from the visual cortices (Burne and Woodward, 1983). Overall, the petrosal lobules of the cerebellum in euarchontoglirans appear to play a significant role in an animal's ability to regulate eye movements to maintain a clear image of a moving object.

Some research has suggested that the large fossae, and therefore lobules, possessed by birds and pterosaurs reflect adaptive specialization to flight (Witmer et al. 2003; but see Walsh et al., 2013) with connections drawn between fossa/lobule size and ecology within birds (Ferreira-Cardoso et al., 2017). Within mammals, however, support for this connection has varied. Analysis of fossil and extant rodent endocasts by Bertrand and colleagues identified a trend toward smaller petrosal lobules in progressively more fossorial sciuroids (Bertrand et al., 2018; 2021) as well as a marked increase in lobular size in early arboreal squirrels (Bertrand et al. 2017; 2021). Conversely, analysis by Ferreira-Cardoso and colleagues (2017) found that, in a diverse sample of primarily extant mammals, ecological variables could not explain variation in fossa/lobule size, and variation was primarily attributed to phylogenetic influence. The contrasting perspectives offered by these analyses, and the potential usefulness of the fossa and associated brain structure if added to our current repertoire of brain features that can be measured in fossil endocasts, necessitates further examination.

The purpose of this study is to perform such an examination on a large dataset of virtual endocasts from closely related species (Superorder Euarchontoglires [Primates, Scandentia, Dermoptera, Rodentia, Lagomorpha]) to determine if ecology influences petrosal lobule scaling patterns. Specifically, this paper seeks to evaluate 1) the scaling relationship between petrosal

lobule size relative to the size of the rest of the endocranium, and to body size, 2) the impact of phylogeny on relative petrosal lobule size, and 3) the influence of ecological behaviors on relative petrosal lobule size within a phylogenetically constrained group of mammals. If the results indicate that ecology plays a significant role in petrosal lobule scaling (as measured from the size of the subarcuate fossa), then these structures may be used to help interpret endocranial morphology of fossil endocasts for this group from the perspective of sensory ecology.

2 | MATERIALS AND DATA COLLECTION

Endocasts of 140 extant euarchontoglirans, including lagomorphs (15), primates (38 = Haplorhini [18], Strepsirrhini [20]), rodents (71 = Squirrel-related clade [27], Ctenohystrica [17], Mouse-related clade [27]), scandentians (14), and dermopterans (2) (Table 1; Figure 3) were used. All endocasts were constructed using micro-CT scans of crania. Endocranial volumes and petrosal lobule volumes were taken from the literature for Sciuroidea (Bertrand et al., 2017, 2018, 2019a, 2021), Lagomorpha (López-Torres et al., 2020) and Scandentia (San Martin-Flores, In prep.). Thirty-four of the non-squirrel-related clade rodents, seven lagomorphs, and the two dermopterans were scanned using a high-resolution X-ray micro-CT scanner at the Shared Materials Instrumentation Facility (SMIF), Duke University (North Carolina). Specimens were loaned from the American Museum of Natural History (AMNH). The micro-CT scans used to create the endocasts of the remaining species were obtained from Morphosource (see Table S1 for detailed information about provenance, scanning locations, scanning parameters for all specimens). Crania were primarily chosen based on neurocranial completeness irrespective of sex. While sex may be a factor influencing brain size and shape, especially for anthropoids, the primates included in this sample exhibit little sexual dimorphism (Fleagle, 2013; Astride et al., 2015). Only adults were included in this analysis, age was determined using dental eruption. The

primate sample used for these analyses was limited to strepsirrhines and platyrrhines. This is because the subarcuate fossa does not scale linearly relative to brain volume in cercopithecoids as it does in strepsirrhines and platyrrhines, and is almost completely absent, expect for a small depression, in many catarrhines including great apes and humans (Gannon et al., 1988).

Virtual endocasts were produced using the X-ray CT scanned images of each cranium. Segmentation of the endocrania was performed in AVIZO® 9.1.1 software (Visualization and Sciences Group, 1995-2020) using a WACOM Cintiq 21UX tablet. The virtual endocasts were manually segmented using the Avizo program by "closing" the endocranial area of a given slice (i.e., tracing a straight line between two bones to separate the endocast from openings for the passage of vessels and/or nerves entering or exiting the endocranium). When the number of slices in the frontal plane exceeded 1800, one of two methods were used: 1) the interpolate tool was used to fill in the endocranial area between two completed slices, with one to four slices separating them; 2) the file size was reduced using ImageJ (Rasband, 1997-2018) to create a version of the dataset that included every other slice (in the frontal plane), thereby increasing the interslice distance in this dimension by two (see Table S1). These methods were used to decrease segmentation time and loading times of large data files without sacrificing the quality of the endocranial reconstruction.

The entire virtual endocast, including the petrosal lobules, was segmented in the frontal plane. The lobules were then segmented independently in the transverse plane, as it is easier to determine the point at which they can be most accurately isolated from the rest of the endocast in this plane. Petrosal lobules were separated from the rest of the endocast by drawing a straight line across the narrowest point at the opening of the subarcuate fossa, manually closing off the fossa from the rest of the endocast (Figure 4). In some sections identifying the narrowest point

was not possible. In these cases, the petrosal lobules were isolated by tracing a straight line between the edges of the anterior semicircular canal, which occurs on either side of the fossa (Figure 4). This was done to ensure the most consistent segmentation across taxa, accounting for variation in the configuration of the subarcuate fossa. Once isolated, the left and right petrosal lobules were each assigned a distinct label-field module. Volumes (mm^3) were calculated in Avizo using the Surface Area Volume module which calculates the volume enclosed in a given surface area for both the left and right petrosal lobules and for the entire endocast. The left and right petrosal lobule volumes were then summed to form the total volume of the lobules. Body masses for each species were derived from order or suborder specific equations using cranial measurements (Table 2). No equations have been published to estimate body mass for scandentians or dermopterans. Consequently, species mean body masses from Sargis (2002) were used for Scandentia. The body masses for *Tupaia javanica*, and *Tupaia belangeri* were provided by EJ Sargis (personal communication). Body masses for the dermopterans were obtained from Stafford and Szalay (2000). All cranial measurements were taken digitally using the Avizo 3D measurement tool.

2.1 | ECOLOGICAL CATEGORIZATION

Species were assigned to primary ecological categories based on their behaviors for activity period, locomotor behavior, and diet (Table 1; see S2 for sources for ecological behaviors). For each primary ecological category, species were then placed into high, medium, and low clustered ecological categories based on the hypothesized demands their ecological behaviors present to the visual and vestibular systems. It was necessary to use this approach to reduce the number of groups being compared to make it possible to run an Ornstein-Uhlenbeck model (described below), which requires there to be more datapoints (taxa) within each category

than there are categories (Butler and King, 2004). Regarding activity pattern, diurnal taxa (n = 56) were placed in the high cluster, crepuscular (n = 10) and cathemeral (n = 6) taxa were placed in the medium cluster, and nocturnal (n = 63) and highly fossorial (n = 5) taxa were placed in the low cluster. These subcategories were created based on the observation that diurnality is more often associated with visual specialization both optically (Veilleux and Kirk, 2013) and neurally (Barton, 1996; 1998; Kirk 2006; Campi and Krubitzer, 2010) and as a result, these taxa may require the greater image stabilization afforded by larger petrosal lobules than taxa which operate in lower light conditions.

High, medium, and low clusters were also applied to locomotor modes and dietary primary ecological categories. For locomotion, arboreal (n = 46) and gliding (n = 10) taxa were placed in the high locomotor cluster, as they navigate through complex three-dimensional, dynamic, and pliant substrates, which present challenges to the visual and vestibular systems. Saltatorial (n = 13), scansorial (n = 13), semi-aquatic (n = 4), and slow arboreal (n = 6) taxa were sorted into the medium locomotor cluster as they engage in behaviors (i.e. bounding, climbing, swimming) which present some challenge to the visual and vestibular systems, but unlike the arboreal and gliding species, they engage in frequent terrestrial, two-dimensional locomotion, or slow deliberate movement which may require fewer visual and vestibular adjustments (Spoor et al., 2007). Finally, terrestrial (n = 36) and fossorial (n = 10) taxa were placed in the low locomotor cluster, as they engage in locomotor behaviors which present less of a stabilization challenge to the visual and vestibular systems relative to the other clusters. Though cursorial taxa (n = 2) are terrestrial, due to their rapid movements and sudden changes in redirection they were placed in the high locomotor cluster with gliding and arboreal taxa.

Lastly, species were sorted into three dietary clusters based on the potential complexity of information presented to the visual and vestibular systems involved in foraging or procuring each food item. Faunivorous (n = 20) and omnivorous (n = 33) taxa were sorted into the high dietary cluster, as capturing animal prey is often associated with visual specializations including higher visual acuity (Veilleux and Kirk, 2014) and greater orbital convergence (Ross, 1995; Barton 2004; Ross et al., 2007; Heesy, 2008), which are dependent on precise control of eye movements. Frugivorous (n = 16), granivorous (n = 11), and gummivorous (n = 3) taxa were placed in the medium dietary cluster. One of the challenges shared by these three ecological behaviors is that their food sources are unevenly distributed over a large area (Mace et al., 1981; Melin et al., 2014) and are often dispersed amongst foliage (Melin et al., 2014). Analysis of the dietary habits of gummivorous primates indicate that feeding occurs on select species which may be patchily distributed (Nash, 1986). These foraging challenges also apply to frugivorous foraging, challenges which are frequently cited as one of the driving forces in the evolution of colour vision amongst frugivorous primates (e.g., Melin et al., 2014; Regan et al., 2001). Fewer analyses have been conducted on the specific foraging challenges associated with seed predation, but granivory is akin to frugivory as seed production is not continuous and is also distinct from folivory as seeds are inconspicuous once dispersed (Janzen, 1971). These ecological foraging behaviors would not be expected to be as visually or vestibularly demanding as omnivory or faunivory, but procurement of these food sources represents more of a challenge in terms of visual location of a given food item when compared to folivores (n = 22), and generalist herbivores (n = 35), which were placed in the low dietary cluster as the relevant food sources are more ubiquitous and readily attainable (Mace et al., 1981).

2.2 | DATA ANALYSIS

All statistical analyses were performed in R 4.0.2 (R Core Team, 2020). Quantitative variables, including petrosal lobule volume (mm^3), endocranial volume minus petrosal lobule volume (mm^3) (hereafter referred to as "Adjusted Endocranial Volume" or AEV), petrosal lobule mass (g), and body mass (g) minus petrosal lobules mass (g) (hereafter referred to as "Adjusted Body Mass" or ABM), were log transformed prior to statistical analysis. The independent variables, AEV and ABM, were used to avoid comparing lobule size to itself in regression analyses. Petrosal lobule volumes in mm^3 were multiplied by 1.036 to convert them to mass using the tissue conversion from Stephan and Colleagues (1981). Values were then converted to grams and used in analyses of petrosal lobule mass and ABM.

Both ordinary least squares (OLS) (package: RRPP, version: 0.6.1, function: lm.rrpp, Collyer and Adams, 2016) and phylogenetic generalized least-square (PGLS) simultaneously estimated with phylogenetic signal in the residual error as Pagel's lambda (package: phylolm, function: phylolm, version: 2.6.2, Ho et al., 2016) analyses were performed to evaluate the scaling patterns of the petrosal lobules relative to endocranial volume and body mass within the sample of euarchontoglirans. Both body mass and endocranial volume were included as independent variables. Body mass was included as some taxa are known to have large brains relative to body mass, which may affect the size of the lobules relative to endocranial volume if the lobules are not also correspondingly large (i.e., if brain expansion occurred in other regions but not the lobules). For instance, anthropoids have exceptionally large brains for their body masses (Jerison 1973), which has been argued to be primarily related to neocortical expansion (Kaas, 2012), and so would not necessarily be reflected in the size of the lobules.

Trees used for phylogenetic analyses were generated from the online vertebrate phylogeny database, vertlife.org (2020), using the subsetting tool. Mammalian phylogenies from

this resource were produced using a "backbone-and-patch" Bayesian method from genetic and fossil data (Upham et al., 2019a,b). For this sample of 140 euarchontoglirans, 10,000 fossil calibrated node-dated credible trees were generated and downloaded. From this posterior distribution of phylogenies, a single tree was obtained using maximum clade credibility function (`maxCladeCred`) from the R package phangorn (version: 2.5.5, Schliep, 2011).

Ordinal scaling patterns were examined using the residuals from the OLS regression analysis of petrosal lobule volume plotted against AEV and petrosal lobule mass plotted against ABM. An analysis of variance (ANOVA) using a randomized residual permutation procedure (rrpp) with 1000 iterations was performed to examine significant differences among orders. An additional ANOVA was performed with primates divided into the suborders (Haplorhini and Strepsirrhini) to assess differences in relative lobule size within Primates, given that anthropoids tend to have larger brains relative to body mass than their strepsirrhine relatives. The PGLS models were run using Pagel's λ correlation structure (Freckelton et al., 2002) for Euarchontoglires overall, and rodents and primates separately (package: phylolm, version: 2.6.2, Ho et al., 2016). The phylogenetic signal of the residuals obtained from the relationship between petrosal lobule volume and AEV and the relationship between petrosal lobule mass and ABM was assessed using Pagel's λ (Pagel, 1999; Freckleton et al., 2002).

To evaluate whether relative lobule size differed between ecological groups, a phylogenetic ANOVA (pANOVA) was performed on residuals from PGLS analyses of petrosal lobule volume and AEV, and petrosal lobules mass and ABM (package: RRPP, version: 0.6.1, functions: `lm.rrpp`, `anova`, Collyer and Adams, 2016) according to the primary ecological categories for each ecological group (i.e. locomotor behaviors, activity pattern, diet) using a brownian motion covariance matrix. This analysis was also repeated on rodents and primates

separately given the differences between the two orders in terms of the functional components of the brain which comprise the lobules and in light of the extreme ecological diversity of rodents, factors which may produce distinct ecological scaling patterns in each order. For the ANOVAs which identified significant differences between ordinal and ecological categories, a post-hoc pairwise comparison was performed using the function `pairwise` from the RRPP R package (Collyer and Adams, 2016) to examine the significance of differences among specific groups. The hypothesis that locomotor behavior, activity pattern, and diet influenced the evolution of relative petrosal lobule size was tested using generalized evolutionary models (Hansen 1997; Butler and King 2004). The first model fit was a single-rate Brownian motion model (BM1) that models how the variance of relative petrosal lobule size accumulates proportionally to evolutionary time under a random walk. The second model fit was a single-peak Ornstein-Uhlenbeck model (OU1) that constrains relative petrosal lobule size to evolve towards one optimum. The BM1 and OU1 models serve as null hypotheses that relative petrosal lobule size does not differ between ecological groups. The last three models fit were multi-peak Ornstein-Uhlenbeck models (OUM) that allowed locomotor behavior (OUMloc), activity pattern (OUMact), and diet (OUMdiet) to exhibit different adaptive optima. All models were fit using the `OUwie` function in the R package OUwie (version: 2.6, Beaulieu et al. 2012) across 1,000 stochastically mapped trees to take into account uncertainty in phylogenetic topology and the ancestral character states. The high, medium, and low clusters (as described above) were used to examine ecology related changes along evolutionary lineages based on the evidence that these clusters are associated with greater challenges to the visual and vestibular system.

Within this modeling analysis, it is expected that species in the high cluster groups will have the largest lobules, and therefore greater capacity for image stabilization, and that species in

the low cluster groups will have the smallest lobules. The evolution of locomotor behavior, activity pattern, and dietary clusters are inferred by performing stochastic character mapping with symmetric transition rates between regimes (Nielsen 2002; Huelsenbeck et al. 2003; Bollback 2006) using the `make.simmap` function in the phytools R package (version: 0.7.47, Revell 2011). Ten stochastic character maps across 100 tree topologies randomly drawn from the posterior distribution of trees were simulated (Upham et al. 2019a,b), resulting in 1,000 character maps for each set of locomotor behavior, activity pattern, and dietary regimes. Relative support for each of the five models was assessed through computation of small sample corrected Akaike weights (AICcW). All models with $\Delta AICc < 2$ were considered to be supported by the data (Burnham and Anderson, 2004). Using the residuals from regression analyses for lobule volume/mass plotted against AEV and ABM, ancestral character states for lobule size were estimated using maximum likelihood with the `fastAnc` function from the phytools package (version: 0.7.47, Revell, 2012) as a heuristic tool to help visualize differences in relative lobule size across lineages.

Phylogenetic ANOVAs were also run on log endocranial volume and log body mass to evaluate the possible relationship between the ecological variables (locomotor behavior, diet, and activity pattern) and total endocranial volume and body mass respectively which may influence the results of petrosal lobule analysis (package: RRPP, version: 0.6.1, functions: lm.rrpp, anova, Collyer and Adams, 2016).

3 | RESULTS

Volumetric analysis indicates that on average petrosal lobules occupy 1.15% of the total endocranial volume. Within this sample, *Coendou prehensilis,* (a nocturnal, arboreal caviomorph

rodent) has the relatively smallest petrosal lobules, at 0.02% endocranial volume and *Ochotona princeps* (a diurnal, terrestrial lagomorph) has the relatively largest at 3.4% endocranial volume. Both OLS and PGLS regression of volumetric data (petrosal lobule volume plotted against AEV) indicate a significant positive linear relationship between the two variables, with AEV accounting for 61.5% ($p = 0.001$) and 60% ($p = < 0.000$) of the variation in petrosal lobule volume respectively (Table 3). Similar results were obtained from the mass OLS and PGLS regression analyses (petrosal lobule mass plotted against ABM) in which there is a significant positive linear relationship between the two variables (Table 3). However, ABM accounted for less of the variation in petrosal lobule mass at 52.4% ($p = <0.000$) for OLS regression and 48.2% ($p = < 0.000$) for PGLS regression.

ANOVA of residuals from the OLS regression of petrosal lobule volume and AEV identified significant differences among ordinal groups (Table 4a). Specifically, the post-hoc pairwise tests indicate that lagomorphs have relatively larger petrosal lobule volumes compared to all other orders (Table 4b; Figure 5a,b), ranging between 1.75% and 3.5% of total endocranial volume. ANOVA of residuals from OLS regression of petrosal lobule mass and ABM (Table 4b) identified significant differences between lagomorphs and both rodents and dermopterans, with lagomorphs having relatively larger lobules. Rodents were significantly different from all other ordinal groups except for dermopterans. However, there was substantial variation in lobule size relative to body mass in rodents (Figure 5c,d). Dermopterans were significantly different from all other ordinal groups (except Rodentia), possessing comparatively smaller lobules relative to ABM. Significant differences were also identified between scandentians and dermopterans, and scandentians rodents, with the former having comparatively larger lobules relative to ABM (Figure 5c,d).

Within primates, haplorhines have significantly smaller petrosal lobules than strepsirrhines relative to AEV (Table 5ab; Figure 5a,b) but not relative to ABM (Table 5a,b; Figure 5c,d), although the ranges of relative petrosal lobule volume and mass between the two groups largely overlap. Overall, Order accounts for 22.1% ($p = 0.001$; Table 4a) of the variation in the residuals of petrosal lobule volume and AEV and 18.2% ($p = 0.001$; Table 4a) of the variation in the residuals of petrosal lobule mass and ABM. As would be expected from this result, both volumetric and mass PGLS analyses identified a strong phylogenetic signal, with Pagel's $\lambda = 0.97$ ($p < 0.001$) for lobule volume relative to AEV analysis and Pagel's $\lambda = 0.95$ ($p < 0.001$) for lobule mass relative to ABM analysis (Table 3). The ancestral state reconstruction documents these lobule scaling patterns across the tree (Figure 6a,b). Relative to both AEV (Figure 6a) and ABM (Figure 6b), lagomorphs, strepsirrhines, scandentians, and sciurid rodents are reconstructed as having evolved proportionately larger petrosal lobules. However, the difference between the haplorhines and strepsirrhines is less marked when considered relative to ABM.

Phylogenetic ANOVAs of relative petrosal lobule volume did not identify significant differences among any of the primary ecological groups in Euarchontoglires (Table 6a; Figure 7), rodents (Table 7), or primates (Table 8). However, phylogenetic ANOVAs of relative petrosal lobule mass identified significant differences among locomotor categories (Table 6b; Figure 7b) within Euarchontoglires. The post-hoc pairwise tests indicate that fossorial taxa had significantly smaller relative lobule masses compared to arboreal, semi-aquatic, slow arborealist, and terrestrial locomotor groups. When pANOVAs of relative lobule mass was performed on rodents separately, no significant differences were detected among any of the primary ecological groups for activity pattern, diet, and locomotor behavior. However, the alpha level for locomotor

behavior was very close to our cut off (0.05) at $p = 0.051$ (Table 7a). Post-hoc tests for relative lobule mass and locomotor behavior in rodents identify significant differences between the fossorial group and arboreal, semi-aquatic, and terrestrial groups (Table S4). Within primates, phylogenetic ANOVAs of relative petrosal lobule volume and mass identified no significant differences among any of the ecological groups (Table 8).

Across Euarchontoglires, the single peak OU1 model (ΔAICc = 0.00, $W_A = 0.48$) and the OUMloc model (ΔAICc = 1.94, $W_A = 0.18$) had the best fit for relative petrosal lobule volume (Table 9a). While the other ecological models (i.e. OUMact, OUMdiet) also had comparable fits, they are just outside of the ΔAICc cut off (ΔAICc = 2.01 and 2.05 respectively; Table 9a). Concerning relative petrosal lobule mass for Euarchontoglires, only the single peak OU1 model was the best-fitted model ($W_A = 0.95$; Table 9b). In rodents, all models (except for OUMdiet) had comparable fits for relative petrosal lobule volume (ΔAICc = 0.00 – 1.66; Table 9a). Only the single peak OU1 model had the best fit for relative petrosal lobule volume mass ($W_A = 0.50$; Table 9b). Though the single peak OU1 models has the lowest ΔAICc values and is therefore best supported among the other models for relative petrosal lobule volume in Euarchontoglires and Rodentia, the fact that all models (except OUMdiet for rodents) had comparable fits (ΔAICc < 2) suggests that there is no single factor among these ecological groups that can account for variation in relative petrosal lobule volume within Euarchontoglires overall or Rodentia. In primates, only the single peak OU1 model had the best fit for relative petrosal lobule volume (Table 9a) whereas the OUMloc and OU1 models had comparable fits for relative petrosal lobule mass (Table 9b). However, parametric bootstrapping of the OUMloc model revealed that the 95% confidence intervals of the theta values overlapped between high, medium, and low clustered locomotor regimes. This indicates that despite the support for the OUMloc model,

variation among these locomotor groups largely overlaps and it is therefore difficult to identify an adaptive pattern associated with locomotor behaviors.

Significant differences in total endocranial volume and body mass were identified between some of the groups for locomotor behavior and diet (Table S3). However, because the differences in total endocranial volume and body mass between locomotor groups are either 1) the result of the small sample size of large bodied and large brained semi-aquatic species or 2) involved a significant degree of overlap between the tested ecological groups, we do not believe that the patterns observed in petrosal lobules size relative to adjusted endocranial volume or adjusted body mass are the result of scaling patterns occurring at the endocranial volume or body mass level.

4 | DISCUSSION

Ordinary least squares regression analysis indicates that there is a strong positive correlation between petrosal lobule size, as determined from the size of the subarcuate fossa, relative to both endocranial volume and body mass in Euarchontoglires. Furthermore, a significant portion of the variation in petrosal lobule size is attributed to variation in endocranial volume and body mass. Analysis of the scaling patterns of the subarcuate fossa in primates and other mammals including Carnivora, Rodentia, Lagomorpha, Marsupialia, and Cetacae presented by Gannon and colleagues (1988) identified a strong positive correlation between subarcuate fossa volume and endocranial volume. Though the statistical methods used by Gannon and colleagues (1988) have been challenged in more recent studies (i.e. Sánchez-Villagra, 2007), their results are largely consistent with those presented here using more rigorous statistical methods and phylogenetic controls.

The result of these analyses differ somewhat from recent analyses performed by Ferreira-Cardoso and colleagues (2017) on petrosal lobule volume from a relatively large sample of mammals (48 species from 13 orders). In this study however, they assessed lobule size relative to total endocranial volume minus lobule volume, and only considered body mass in relation to the residuals from that relationship. Here, lobule size was evaluated relative to both endocranial volume and body mass separately to help parse out differences in lobule scaling for highly encephalized groups (i.e. the platyrrhines). Evaluating lobule scaling relative to these variables independently helped to identify subordinal scaling patterns between strepsirrhines and haplorhines.

4.1| Phylogenetic Signals and Ordinal Patterns

In analyses of relative petrosal lobule volume as determined from subarcuate fossa the volume, lagomorphs had significantly larger lobules compared to all other orders (Figure 5a,b). However, relative to body mass, the petrosal lobules of lagomorphs largely fall within the range of all other orders only significantly differing from Dermoptera and Rodentia, which possess comparatively smaller relative lobule masses (Figure 5c,d). This suggests two possible scenarios for the evolution of the petrosal lobules within Lagomorpha, which are not necessarily mutually exclusive: 1) that there was an increase in the size of the lobules relative to brain/endocranial size within the lagomorph lineage occurring soon after their separation from Rodentia or 2) that there was an increase in the size of the rest of the brain/endocranium (excluding the lobules/subarcuate fossa) in other euarchontogliran groups independently.

The ancestral state reconstruction (ASR) analysis for both relative lobule volume and mass suggests that the lobule size increased within the lagomorph lineage since their common

ancestor with Rodentia, which may suggest that the first option is better supported. However, the ASR analysis was based only on modern data since relevant information from fossil euarchontoglirans is only patchily available. In the absence of data from fossils, these analyses really only constitute a heuristic device that produces hypotheses to be tested with fossil data. Nevertheless, the endocasts of Mesozoic mammals and cynodonts are described as having large petrosal lobules, which indicates that this characteristic may be ancestral for Mammalia (Kielan-Jaworowska, 1986). However, quantitative data have been obtained for a handful of Mesozoic mammals (Macrini, 2006; Macrini et al., 2007a, 2007b; Csiki-Sava et al., 2018) revealing a wide range of values (0.23% to 5.98% of endocrania volume) suggesting that more data is necessary to determine the ancestral condition for placental mammals. Given that lagomorphs are nested within Euarchontoglires, it seems more parsimonious to suggest that this condition is a product of evolutionary changes within that clade. But to consider this question more rigorously, quantitative data for outgroups to Euarchontoglires need to be added.

The only fossil lagomorph for which petrosal lobule data are known is the early Oligocene stem lagomorph, *Megalagus turgidus*, which also possessed large petrosal lobules relative to endocranial volume, similar in size to those of extant leporids, but smaller than extant ochotonids (López-Torres et a., 2020). Significantly, the size of the petrosal lobules relative to endocranial volume in *M. turgidus* are larger than observed in stem rodents and stem primates, which does suggest some shift in the relative size (or relative importance) of this part of the brain in lagomorph evolution. However, extant lagomorphs are reconstructed as having had a lower Encephalization Quotients (EQ) compared to extant rodents, and the EQ was also found to be lower for *M. turgidus* compared to stem rodents (López-Torres et al., 2020). These various lines of evidence suggest that both postulated explanations are likely at work. It appears that the large

size of the petrosal lobules relative to endocranial volume in lagomorphs is being driven in part by their otherwise small brains. But as the brain evolved in lagomorph evolution, the petrosal lobules may have been prioritized when other regions were not, or at least were not to the same degree as in other euarchontogliran clades (e.g., the neocortex, which expanded in lagomorph evolution, but not to the same degree as in Primates or some rodent lineages; Long et al., 2015; Bertrand et al., 2017, 2019a; López-Torres et al., 2020). As such, there may be some ecological basis for this contrast, perhaps related to the saltatory behavior of leporids or need for predator detection in all lagomorphs as prey animals. However, this suggested relationship between lobule size and ecological behaviors within Lagomorpha requires additional testing.

Distinct scaling relationships for relative petrosal lobule volume and mass were also identified within Primates. Specifically, haplorhines had significantly smaller petrosal lobules compared to strepsirrhines relative to endocranial volume (Figure 5a,b). Based the ancestral state reconstruction, it appears that the small relative lobule volumes identified in the strepsirrhines are being driven primarily by the lemuriforms and not the lorisiforms, or at least not to the same extent (although again this observation would benefit from testing with fossils; Figure 6a). However, there is little difference in the size of the lobules relative to body mass between the two suborders (Figure 5c,d; 6b), although there are particular lineages that show evidence of proportional decrease in both relative lobule volume and mass (e.g. *Daubentonia* and *Ateles*). As such, the pattern observed in relation to endocranial volume is likely strongly influenced by the significant expansion of the rest of the brain, primarily in the neocortex, in anthropoids (Jerison 1973; Barton, 1996; Kaas, 2012).

The scaling patterns of the scandentians generally mirror those of the rodents relative to both volume and mass. This is not surprising given the ecological analogies which have been

drawn between them, especially between scandentians and squirrels, and the neural convergences in other visual structures between the two groups (Kaas, 2002). However, relative lobule volumes and masses of the squirrel-related clade are reconstructed as being larger than those of the scandentians (as visualized in the ASR; Figure 6a,b), which would be consistent with evidence from the fossil record that expansion of this part of the brain occurred in sciuroid evolution (Bertrand et al., 2017, 2018, 2021). In contrast, dermopterans have small lobules relative to both endocranial volume and body mass. Although this might be unexpected in arboreal, gliding animals, the small lobules of the dermopterans are consistent with the highly variable and often small lobules reported for gliding rodents (Bertrand et al., 2017, 2021).

The evidence that phylogeny significantly influences petrosal lobule scaling patterns is supported by the strong phylogenetic signal identified in petrosal lobule size relative to both endocranial volume (Pagle's $\lambda = 0.966$) and body mass (Pagle's $\lambda = 0.949$). Ferreira-Cardoso and colleagues (2017) also identified a strong phylogenetic signal in the scaling relationship between petrosal lobule volume and endocranial volume in a smaller but more phylogenetically diverse sample of mammals (Pagle's $\lambda = 0.93$). Based on these results it appears that relative lobule size is strongly influenced by phylogeny across Mammalia (Ferreira-Cardoso et al., 2017) and within Euarchontoglires.

4.2 | Ecological Patterns

It was hypothesized that the subarcuate fossa and correspondingly the petrosal lobules would be larger in taxa which engage in ecological behaviors that place greater demand on the visual and the vestibular systems and smaller in taxa that do not engage in such demanding behaviors. Specifically, the behaviors hypothesized to be more demanding, therefore requiring the greater image stabilization afforded by larger petrosal lobules, include diurnality, arboreality,

and faunivory; and the behaviors hypothesized to be the least demanding included nocturnality, fossoriality, terrestriality, and folivory. Contrary to these predictions, the results presented here suggest that general patterns in ecology, as encapsulated in our scoring system, do not strongly influence variation in the size of the petrosal lobules across Euarchontoglires. While there is stronger support for the ecological models in the Ornstein-Uhlenbeck analysis of clustered groups (i.e. high, medium, low categories) than for the Brownian Motion model across Euarchontoglires for both relative lobule volume and mass, the single peak OU model (OU1) was best supported. This suggests that while ecological factors may influence the evolution of relative lobule size, the ecological clusters used in this study may not effectively capture this variation and/or that other factors not accounted for by these ecological clusters are influencing petrosal lobule evolution in Euarchontoglires. Correspondingly, in nearly all of the pANOVAs, no significant differences were identified between ecological categories for locomotor behavior, diet, and activity pattern. Importantly however, an ecological pattern was identified in the pANOVA with respect to fossorial rodents, which have smaller relative lobule masses compared to several of the other locomotor categories across Euarchontoglires, including the arboreal, semi-aquatic, slow arborealist, and terrestrial groups.

With the exception of the fossorial rodents, these results support comparable analyses performed by Ferriera-Cardoso and colleagues (2017), which found that ecology did not play a role in relative lobule volume in a diverse sample of extinct and extant taxa from across Mammalia. There are several factors that can help to explain the different results obtained here for the fossorial rodents. First, the sample in this study is more phylogenetically constrained and therefore the anatomical structure which forms the lobules are more likely to be homologous between taxonomic groups. Second, in this study there are a greater number of species in each of

the ecological categories, including the fossorial group, allowing for greater resolution of lobular variation for each category. And third, lobule size was evaluated against both endocranial volume *and* body mass whereas Ferriera-Cardoso and colleagues (2017) only assessed lobule size against endocranial volume in ecological analyses. Nevertheless, evaluating lobule scaling patterns relative to both endocranial volume and body mass is valuable given the differences in relative lobule volume and mass identified in certain groups, especially those which are highly encephalized (i.e. anthropoids).

The relationship between relative lobule mass and fossoriality supports recent analyses of petrosal lobule scaling in rodents (Bertrand et al., 2017; 2018; 2021). Analysis using the endocasts of extinct and extant sciuroid rodents identified a marked downgrade in the size of the petrosal lobules relative to both endocranial volume and body mass in progressively fossorial aplodontids (Bertrand et al., 2018). These changes in relative lobule size were attributed to a decrease in visual ability associated with burrowing behavior in the aplodontid lineage (Bertrand et al., 2018). Additionally, analysis of locomotor behavior and brain evolution noted significant differences in the percentage of petrosal lobule volume to endocranial volume between fossorial squirrels and their arboreal relatives (Bertrand et al., 2021), which is consistent with the pattern presented here. Analyses of the inner ear in caviomorph rodents indicate that the subarcuate fossa is larger in taxa which engage in rapid complex movements, as in the semi-aquatic *Myocastor*, and smaller in burrowing taxa, like the fossorial *Ctenomys* (Arnaudo et al., 2020). Outside of neural anatomy, the transition to fossoriality is associated with many cranial (Agrawal, 1967), postcranial (Samuels and Van Valkenburgh, 2008; Wölfer et al., 2019), and soft tissue adaptions (i.e. vibrissae, ear, and tail length; Verde Arregoitia et al., 2016) within rodents appropriate to this unique ecological niche. Likewise, the small relative lobule masses of

the fossorial rodents may therefore reflect a relaxation of adaptive pressure on these visual structures or active selection given the energetic costs of maintaining brain tissue (Williams and Herrup, 1998). Reduced visual reliance has been shown to have profound effects on the brain including the size of the neocortex. Specifically, the visual cortex is reduced in shrews (Catania et al., 1999), echolocating bats (Krubitzer, 1995) and some moles (Catania and Kaas, 1995). In the case of the fossorial rodents, these slow-moving species, which spend a significant part of their lives in low light conditions where olfaction and vibrissal sensing are better suited (Stein, 2000), have a reduced need for precise control of eye movements afforded by larger lobules.

The small relative lobule masses of the fossorial rodents identified in this analysis may ultimately relate to overall brain size, as some fossorial rodents (i.e. *Cryptomys hottentotus*) are known to have smaller brains relative to body mass (Bernard and Nurton, 1992). Fossorial rodents are reported to have smaller lobule volumes relative to endocranial volume compared to other locomotor groups in previous studies (Bertrand et al., 2018; 2021) and appear to have smaller lobule volumes in this analysis as well (Figure 7a). However, no significant differences were identified in relative lobule volume between the fossorial taxa and other locomotor groups in Euarchontoglires more generally, or between relative lobule volume or mass and any ecological variable in the rodents separately. It is likely that the identification of ecological patterns in relative lobule size by Bertrand and colleagues (2018; 2021) was made possible by the inclusion of fossil material and analysis of lobule scaling patterns through time within specific lineages. Additionally, the lack of clear ecological patterns identified in the Ornstein-Uhlenbeck model may relate to the clustering of ecological groups necessary to run the analysis, which may obfuscate the kind of within lineage changes that Bertrand and colleagues (2018, 2021) documented.

The absence of significant differences in relative lobule size between the fossorial rodents and other groups when analyzed in the context of endocranial volume in this analysis may relate to the evolution of digging and fossoriality within Rodentia. Fossoriality has evolved independently several times in different rodent groups (here represented by Bathyergidae, Spalacidae, Aplodontidae) and has produced disparate adaptations in skeletal bone structure (Amson and Bibi, 2021) and skull morphology (Fournier et al., 2021). This disparity is the product of a variety of factors including evolutionary history, soil type, time spent above ground, and significantly, digging behavior (Stein, 2000). For example, *Ctenomys* engages in "scratch-digging" behavior to excavate burrows in which the forelimbs are primarily used to break apart the soil, while its close relative, *Spalacopus*, engages in "chisel-tooth" digging in which large procumbent incisors are used to break up the soil (Stein, 2000). In some species, as in *Ellobius*, the head itself is used in a shoveling motion to excavate tunnels. The diversity of digging behaviors and disparity in fossorial adaptations (Amson and Bibi, 2021; Fournier et al., 2021) may have influenced subarcuate fossa size and therefore lobule size, especially if modifications have been made to the brain case. While it is most likely that the small lobules of these fossorial species relate to their reduced reliance on vision, a feature which characterizes fossorial groups (Stein, 2000), this result, together with previous analyses (Bertrand et al., 2018; 2021) highlights the need for clade specific, fossil informed analyses of fossorial adaptations.

Similar analyses of fossil and extant squirrels identified an increase in the relative size of the lobules between early fossil rodents and the later occurring arboreal stem squirrel, *Cedromus wilsoni* (Bertand et al., 2017; 2021), changes which were attributed to improved vision associated with the transition to arboreality (Bertrand et al., 2017; 2018) or in the very least, which helped to facilitate the transition to arboreality in the squirrel lineage (Bertrand et al.,

2021). These analyses document clear ecological scaling relationships in lobule size when patterns are informed by fossils. Though there may have been changes in the relative size of the petrosal lobules associated with early ecological transitions within Rodentia, specifically with respect to members of the squirrel-related clade (Bertrand et al., 2017; 2018; 2021), no such pattern is identified within the current analysis focused on extant rodents despite the significant variability in relative lobule size and the diversity of ecological behaviors. The analyses by Bertrand and colleagues (2017) on brain variation in fossil and extant squirrels found that they did not possess large lobules relative to endocranial volume and the size of the lobules relative to body mass for *C. wilsoni* were within the range of extant squirrels. Ancestral state reconstruction of lobule size by Bertrand and colleagues (2021) suggests that squirrels had larger lobules prior to their transition to arboreality, which was then followed by an increase in overall brain size as they became more arboreal. As such, this raises the possibility that there may be shifts in lobule size within particular lineages that are being masked at the scale of the current analysis, or by subsequent events in brain evolution.

The absence of an ecological signal in petrosal lobule size is unexpected for primates. The primate visual system is highly specialized for the accurate perception of distance and detail (Dominy et al., 2001), which depend on precise control of eye movements. For instance, compared to other mammals, primates have a high degree of orbital convergence (Ross, 1995; Ross et al., 2007; Heesy, 2004; 2008). The effect of this convergence is that the visual fields seen by each eye overlap significantly (Ross, 1995; Heesy, 2004). The extensive overlap of the visual fields in primates creates a large zone of stereoscopic depth perception (Howards and Rogers, 1995), using the differences between the two images seen by the eyes viewing an object at slightly different angles (Heesy, 2008). Importantly, accurate depth perception and the high

degree of binocular field overlap require precise coordination of the eyes to fuse the two large monocular fields into one image and maintain fixation on an object of interest (Wallace et al., 2013). Additionally, orbital convergence in primates is associated with ecological behaviors, in that faunivorous species tend to have more convergent orbits compared to non-faunivorous species (Heesy, 2008; 2009). Orbital convergence is also positively correlated with the size of the visual structures of the brain, including the lateral geniculate nucleus and the primary visual cortex (Barton, 2004). Furthermore, morphological studies of the primate eye and orbit demonstrate that haplorhine primates have exceptionally high visual acuity (i.e. the ability to make finely detailed differentiations between closely spaced objects) compared to other mammals (Veilleux and Kirk, 2009). Haplorhines also possess a retinal fovea, a pit at the back of the eye with a high density of photoreceptors, where visual acuity is greatest (Kay et al., 1997). Precise control of eye movements is essential for taxa with high visual acuity, especially haplorhines (Kirk and Kay, 2004), where a viewed object must be brought to the fovea to be seen in greatest detail. Analysis of the relationship between visual acuity and the dimensions of the semicircular canals, which provide proprioceptive information also used to regulate eye movements, suggest a strong correlation between the two, such that as visual acuity increases so does the curvature of the canals allowing for more precise perception of the direction and velocity of head and body movements (Kemp and Kirk, 2014). Given 1) that the visual adaptations possessed by primates, including orbital convergence and high visual acuity are predicated on precise control of eye movements, 2) the evidence that visual specializations are known to influence the size of the brain, neocortex, and specific visual structures, and 3) the connection between visual acuity and the semicircular canals, it is surprising that the lobules, which regulate smooth pursuit and velocity of eye, are not correspondingly large within

primates, even relative to body size. Instead, lagomorphs, with low orbital convergence (Heesy, 2004) and low expected acuity as herbivores (Veilleux and Kirk, 2009), possess the largest lobules, at least relative to endocranial volume.

Though these results are unexpected, there are some possible explanations as to why no ecological signal was identified in the size of the petrosal lobules within Primates, especially considering the uncertainty surrounding the specific function of the tissues which fill the subarcuate fossa in these groups. Despite the evidence that the lobules play a significant role in the control of eye movements (Hiramatsu et al., 2008) they are not the only part of the brain which performs this function. As mentioned, the petrosal lobules are part of a functional unit, the floccular-parafloccular complex of the vestibulocerebellum, which regulates VOR, stabilizes the eyes, and controls the velocity of eye movements (Zee et al., 1981; Shojaku et al., 1990; Nagao, 1992; Rambold et al., 2002; Hiramatsu et al., 2008: Ilg and Their, 2008). Though the petrosal lobules of primates are specifically involved with the control of smooth pursuit eye movements, this function is also performed by the ventral paraflocculus (Nagao, 1992; Nagao et al., 1997), which sits outside the fossa. While some parts of the complex may perform more specific functions, the anatomical divisions within the primate floccular-parafloccular complex do not reflect functional separations (Noda and Mikami, 1986).

Furthermore, it is worth noting that most of the analyses that assess the function of the petrosal lobules are based on macaques. Catarrhines are known to have smaller lobules that do not scale linearly with body mass, as they do in other mammals and primates (Gannon, et al., 1988). Considering the systematic reduction in lobular size within this lineage it is perhaps not surprising there is little functional compartmentalization in the catarrhine petrosal lobule. With hominids lacking the lobules and the fossa entirely (Gannon et al., 1998), other parts of the

cerebellum have presumably taken on the functional role of this structure long before its disappearance. As a result, functional conclusions drawn from the catarrhine brain may not be applicable to the petrosal lobules of strepsirrhines and platyrrhines, in which the lobules are comparatively large (Gannon et al., 1988).

What's more, it is also somewhat problematic to infer the specifics of petrosal lobule function in rodents using the morphologically derived macaques. In haplorhine primates, concerted eye movements are essential for binocular fusion and centering an object of interest on the fovea of each eye (Wallace et al., 2013). Analysis of eye movements in the rat, however, indicate that the left and right eye do not move in a concerted fashion, precluding the possibility of primate-like binocular fusion (Wallace et al., 2013). Instead, a field of binocular overlap is maintained over the animal's head despite variation in the alignment of the eyes and rapid movements of the head and body (Wallace et al., 2013). In small mammals like the rat, the most important function of the visual system is the detection of predators at a distance (Wallace et al., 2013; Land, 2013; De Franceschi et al., 2016), as location of food and navigation of substrates can be achieved through olfaction and vibrissae (Kleinfeld et al., 2006; Hollander et al., 2012). If concerted control of eye movements, which the petrosal lobules play a role in regulating, is not an integral component of rodent visual behavior, and the regulation of eye movements is primarily related to predator detection, then there may not be a relationship between the size of the lobules and locomotor behaviors, diet, or activity pattern. There may instead be a relationship between anti-predator visual behavior and the size of neural structures regulating eye movements. For example, ochotonids are noted for having large lobules relative to brain size, even larger than in the saltatorial leporids (López-Torres et al., 2020). This group of small terrestrial mammals often lives in rocky open environments which exposes them to both aerial

and terrestrial predators (Ivins and Smith, 1983; Holmes, 1991). Precise and rapid eye movement for predator detection may be imperative to identify and alert colony members of potential threats (Ivins and Smith, 1983; Volodin et al., 2018) necessitating larger lobules in this group.

Some research has also identified a neural connection between the auditory cortex and the floccular-paraflocular complex of rodents (Azizi et al., 1985; Azizi and Woodward, 1990; Du et al., 2017). In electrical stimulation experiments on the rat brain, approximately 33% of the neurons in the paraflocculi were responsive to stimulus of the auditory cortex (Azizi et al., 1985) and 71.4% of neurons in the contralateral auditory cortex were responsive to stimulus in the parafloculus (Du et al., 2017). The functional significance of this connection is unknown, but a feedback loop between the two structures is suggested to play a role in tinnitus in humans (Du et al., 2017; Mennink et al., 2020). At present, no studies have attempted to examine both visual and auditory roles of the parafloculus, and doing so is likely to be exceedingly difficult as categorizing animals based on auditory requirements would require even more speculation than doing so based on visual requirements. But that does not mean that such patterns do not exist.

The absence of a relationship between petrosal lobule size and ecology (with the exception of the fossorial rodents) could also relate to constraints on fossa expansion within the cranium. The semicircular canals surround the subarcuate fossa and scale according to body mass and locomotor agility (Jeffery et al., 2008; Spoor et al., 2007)—the petrosal lobules may be constrained to some degree by the size of these canals. However, the limited relationship between locomotor behavior and lobule/fossa size in this analysis negates the suggestion that the fossa scales solely as a product of changes in semicircular canal size. From an ontogenetic perspective, the subarcuate fossa is not formed via ossification of tissue surrounding the petrosal lobules. Instead, the formation of the subarcuate fossa is connected to the growth and

development of the semicircular canals, and the petrosal lobules secondarily occupy the fossa (McClure and Daron, 1971; Jeffery and Spoor, 2006). Though the fossa and the canals are developmentally connected (Jeffery and Spoor, 2006), the size of the fossa does not appear to be entirely dependent on the size of the canals. Other factors related to cranial scaling may have a significant impact on fossa and lobular scaling. For example, locomotor behavior is suggested to play a role in cranial (Lu et al., 2014) and endocranial shape (Bertrand et al., 2019b) in squirrels. This may relate to the small lobules of gliding squirrels as they possess a large auditory bulla which may limit the space available for the fossa (Bertrand et al., 2019b). Despite the prospective importance of visual tracking in arboreal and volant locomotion, some gliding rodent species lack the lobules entirely (i.e. *Petinomys setosus*; Bertrand et al., 2017). Furthermore, species with globular crania (i.e. hominoids) also do not possess a subarcuate fossa, which is presumably related to factors other than ecology.

5 | CONCLUSION

In this paper, the scaling patterns of the petrosal lobules, as determined from endocranial reconstructions of subarcuate fossa size, were examined in 140 extant euarchontoglirans to evaluate scaling relationships with the rest of the endocranium and with body mass to identify phylogenetic patterns and to determine if ecological factors play a role in the relative sizes of these structures using phylogenetically controlled analyses. These analyses indicate that the size of the petrosal lobules is positively correlated with both endocranial volume and body mass, which is largely consistent with previous research (Gannon et al., 1988; Ferreira-Cardoso et al., 2017). Overall, phylogeny appears to be a major factor in the scaling of the petrosal lobules, with significant differences in relative petrosal lobule size identified between orders and suborders.

Specifically, lagomorphs had significantly larger petrosal lobules compared to all other orders relative to endocranial volume and haplorhines had significantly smaller petrosal lobules compared to strepsirrhines relative to endocranial volume. The ordinal scaling patterns identified in petrosal lobule size relative to endocranial volume differed to some degree from those identified in petrosal lobule mass relative to body mass. The relative lobule mass of the lagomorphs was only significantly different from the rodents and the dermopterans, while no difference was identified between haplorhine and strepsirrhine relative lobule masses. These contrasts highlight the importance of doing both types of comparisons, since they offer different perspectives on the evolutionary process. Rodents were also found to be significantly different from all other groups, except for dermopterans, in relative lobule mass, but this pattern is difficult to characterize given the range of variation for relative lobule mass in this group. These contrasting results imply a complex interplay between the evolution of the size of the petrosal lobules with the evolution of body mass and relative brain size.

While there is evidence that the unique scaling patterns identified in several of these phylogenetic groups may have been ecologically driven early in their respective lineages (Bertrand et al., 2017; 2018; 2019b; 2021), no connection was identified between most of the ecological factors tested here and relative lobule size within this sample of extant taxa. However, significant differences in lobule size were identified for fossorial taxa in relative lobule mass across Euarchontoglires, as the fossorial taxa, comprised exclusively of rodents, had small lobules compared to arboreal, scansorial, semi-aquatic, slow arborealist, and terrestrial groups. Small lobules and subarcuate fossae have been documented in other studies of fossorial aplodontiids and ischyromyids (Bertrand et al., 2018; 2021) and caviomorphs (Arnaudo et al., 2020). Together these results indicate that the small lobules in fossorial rodents may reflect an

adaptation to burrowing or in the least a relaxation of selective pressure, where the need for larger lobules and increased coordination of eye movements is decreased relative to other locomotor behaviors.

The lack of a relationship identified between relative lobule size and other ecological factors may be influenced by differences in the functional anatomical organization among groups of the lobules (i.e. between Primates and Glires), which necessitates a more phylogenetically constrained analysis than has been presented here. Furthermore, it is possible that adaptive changes to the petrosal lobules occurred early in these lineages, but that subsequent changes may have obscured those patterns in the extant sample, as suggested by the contrast between the results here and those found in the study of fossil sciuroids and ischyromyids (Bertrand et al., 2017, 2018, 2021). The underlying goal of this study was to better understand the scaling relations of the petrosal lobules in Euarchontoglires, with the hope that the results may be applied in analyses of fossil endocasts to better understand the sensory repertoire of extinct species. As ecology related scaling patterns appear only in fossorial taxa within this extant sample it is difficult to draw clear-cut conclusions about the significance of lobule size in fossil specimens outside of this ecological category. As a result, the extent to which variation in these lobules and the subarcuate fossa can be used to interpret the morphology and sensory ecology of fossil taxa is limited and needs to be tested within specific clades and in the context of considering evolutionary trajectories (informed by fossil material) for both overall brain size and body mass.

Acknowledgments

We would like to acknowledge Dr. P. Cox, Dr. A. Harrington, Dr. R. Asher, and Dr. M. Lowe for access to CT scans through the Morphosource database. We thank Dr. E. Sargis for his communications on scandentian body masses. We would also like to thank the work/study students, Koda MacLellan, Pamela Santos, Tejnarine Persaud, and James Graves for their efforts in creating endocasts for this project.

Accessibility

All endocasts used for this analysis will be made available on Morphosource in the following project: https://www.morphosource.org/projects/000424317?locale=en.

Petrosal Lobule Paper References (APA Format - organized alphabetically)

Amson, E., & Bibi, F. (2021). Differing effects of size and lifestyle on bone structure in mammals. *BMC biology, 19*(1), 1-18.

Agrawal, V. C. (1967). Skull adaptations in fossorial rodents. *Mammalia 31*, 300–312.

Arnaudo, M. E., Arnal, M., & Ekdale, E. G. (2020). The auditory region of a caviomorph rodent (Hystricognathi) from the early Miocene of Patagonia (South America) and evolutionary considerations. *Journal of Vertebrate Paleontology*, *40*(2), e1777557.

Azizi, S. A., Burne, R. A., & Woodward, D. J. (1985). The auditory corticopontocerebellar projection in the rat: inputs to the paraflocculus and midvermis. An anatomical and physiological study. Experimental brain research, *59*(1), 36-49.

Azizi, S. A., & Woodward, D. J. (1990). Interactions of visual and auditory mossy fiber inputs in the paraflocculus of the rat: a gating action of multimodal inputs. *Brain research*, *533*(2), 255-262.

Balanoff, A. M., & Bever, G. S. (2020). The role of endocasts in the study of brain evolution. In J.H. Kaas (Eds.), *Evolutionary Neuroscience* (pp. 29-49). Academic Press.

Barks, S. K., Calhoun, M. E., Hopkins, W. D., Cranfield, M. R., Mudakikwa, A., Stoinski, T. S., Patterson, F. G., Erwin, J. M., Hecht, E. E., Hof, P. R., & Sherwood, C. C. (2015). Brain organization of gorillas reflects species differences in ecology. *American journal of physical anthropology, 156*(2), 252-262.

Barton, R. A., Purvis, A., & Harvey, P. H. (1995). Evolutionary radiation of visual and olfactory brain systems in primates, bats and insectivores. *Philosophical Transactions of the Royal Society of London. Series B: Biological Sciences*, *348*(1326), 381-392.

Barton, R. A. (1996). Neocortex size and behavioral ecology in primates. *Proceedings of the Royal Society of London. Series B: Biological Sciences*, *263*(1367), 173-177.

Barton, R. A. (1998). Visual specialization and brain evolution in primates. *Proceedings of the Royal Society of London. Series B: Biological Sciences*, *265*(1409), 1933-1937.

Barton, R. A. (2004). Binocularity and brain evolution in primates. *Proceedings of the National Academy of Sciences*, *101*(27), 10113-10115.

Barton, R. A. (2006). Primate brain evolution: integrating comparative, neurophysiological, and ethological data. *Evolutionary Anthropology: Issues, News, and Reviews: Issues, News, and Reviews*, *15*(6), 224-236.

Barton, R. A., & Harvey, P. H. (2000). Mosaic evolution of brain structure in mammals. *Nature*, *405*(6790), 1055-1058.

Beaulieu, J. M., Jhwueng, D. C., Boettiger, C., & O'Meara, B. C. (2012). Modeling stabilizing selection: expanding the Ornstein–Uhlenbeck model of adaptive evolution. *Evolution: International Journal of Organic Evolution*, *66*(8), 2369-2383.

Belton, T., & McCrea, R. A. (2000a). Role of the cerebellar flocculus region in cancellation of the VOR during passive whole body rotation. *Journal of neurophysiology*, *84*(3), 1599-1613.

Belton, T., & McCrea, R. A. (2000b). Role of the cerebellar flocculus region in the coordination of eye and head movements during gaze pursuit. *Journal of neurophysiology*, *84*(3), 1614-1626.

Bernard, R. T. F., & Nurton, J. (1992). Ecological correlates of relative brain size in some South African rodents. *South African Journal of Zoology*, *28*(2), 95-98.

Bertrand, O. C., Amador-Mughal, F., & Silcox, M. T. (2017). Virtual endocast of the early Oligocene *Cedromus wilsoni* (Cedromurinae) and brain evolution in squirrels. *Journal of anatomy*, *230*(1), 128-151.

Bertrand, O. C., Amador-Mughal, F., Lang, M. M., & Silcox, M. T. (2018). Virtual endocasts of fossil Sciuroidea: brain size reduction in the evolution of fossoriality. *Palaeontology*, *61*(6), 919-948.

Bertrand, O. C., Amador-Mughal, F., Lang, M. M., & Silcox, M. T. (2019a). New virtual endocasts of Eocene Ischyromyidae and their relevance in evaluating neurological changes occurring through time in Rodentia. *Journal of Mammalian Evolution*, *26*(3), 345-371.

Bertrand, O. C., San Martin-Flores, G., & Silcox, M. T. (2019). Endocranial shape variation in the squirrel-related clade and their fossil relatives using 3D geometric morphometrics: contributions of locomotion and phylogeny to brain shape. *Journal of Zoology*, *308*(3), 197-211.

Bertrand, O. C., Püschel, H. P., Schwab, J. A., Silcox, M. T., & Brusatte, S. L. (2021). The impact of locomotion on the brain evolution of squirrels and close relatives. *Communications biology*, *4*(1), 1-15.

Bhatnagar, K. P., & Kallen, F. C. (1974). Cribriform plate of ethmoid, olfactory bulb and olfactory acuity in forty species of bats. *Journal of Morphology*, *142*(1), 71-89.

Bollback, J. P. (2006). SIMMAP: stochastic character mapping of discrete traits on phylogenies. *BMC bioinformatics*, *7*(1), 1-7.

Burne, R. A., & Woodward, D. J. (1983). Visual cortical projections to the paraflocculus in the rat. *Experimental brain research*, *49*(1), 55-67. bur

Burnham, K. P., & Anderson, D. R. (2004). Multimodel inference: understanding AIC and BIC in model selection. *Sociological methods & research*, *33*(2), 261-304.

Butler, M. A., & King, A. A. (2004). Phylogenetic comparative analysis: a modeling approach for adaptive evolution. *The American Naturalist*, *164*(6), 683-695.

Campi, K. L., & Krubitzer, L. (2010). Comparative studies of diurnal and nocturnal rodents: differences in lifestyle result in alterations in cortical field size and number. *Journal of Comparative Neurology*, *518*(22), 4491-4512.

Catania, K. C., & Kaas, J. H. (1995). Organization of the somatosensory cortex of the star-nosed mole. *Journal of Comparative Neurology, 351*(4), 549-567.

Catania, K. C., Lyon, D. C., Mock, O. B., & Kaas, J. H. (1999). Cortical organization in shrews: evidence from five species. *Journal of Comparative Neurology, 410*(1), 55-72.

Clutton-Brock, T. H., & Harvey, P. H. (1980). Primates, brains and ecology. *Journal of zoology*, *190*(3), 309-323.

Collyer, M. L., & Adams, D. C. (2018). RRPP: An r package for fitting linear models to high-dimensional data using residual randomization. *Methods in Ecology and Evolution*, *9*(7), 1772-1779.

Csiki-Sava, Z., Vremir, M., Meng, J., Brusatte, S. L., & Norell, M. A. (2018). Dome-headed, small-brained island mammal from the Late Cretaceous of Romania. Proceedings of the National Academy of Sciences, 115(19), 4857-4862.

De Franceschi, G., Vivattanasarn, T., Saleem, A. B., & Solomon, S. G. (2016). Vision guides selection of freeze or flight defense strategies in mice. *Current biology*, *26*(16), 2150-2154.

de Winter, W., & Oxnard, C. E. (2001). Evolutionary radiations and convergences in the structural organization of mammalian brains. *Nature*, *409*(6821), 710-714.

DeCasien, A. R., Williams, S. A., & Higham, J. P. (2017). Primate brain size is predicted by diet but not sociality. *Nature ecology & evolution*, *1*(5), 1-7.

DeCasien, A. R., & Higham, J. P. (2019). Primate mosaic brain evolution reflects selection on sensory and cognitive specialization. *Nature ecology & evolution*, *3*(10), 1483-1493.

Dominy, N. J., Lucas, P. W., Osorio, D., & Yamashita, N. (2001). The sensory ecology of primate food perception. *Evolutionary Anthropology: Issues, News, and Reviews: Issues, News, and Reviews*, *10*(5), 171-186.

Du, Y., Liu, J., Jiang, Q., Duan, Q., Mao, L., & Ma, F. (2017). Paraflocculus plays a role in salicylate-induced tinnitus. *Hearing research*, *353*, 176-184.

Dunbar, R. I. M. (1992). Neocortex size as a constraint on group size in primates. *Journal of human evolution*, *22*(6), 469-493.

Dunbar, R. I. M. (1995). Neocortex size and group size in primates: a test of the hypothesis. *Journal of human evolution*, *28*(3), 287-296.

Dunbar, R. I. M., & Shultz, S. (2007). Understanding primate brain evolution. *Philosophical Transactions of the Royal Society B: Biological Sciences*, 362(1480), 649-658.

Eisenberg, J. F., & Wilson, D. E. (1978). Relative brain size and feeding strategies in the Chiroptera. *Evolution*, 740-751.

Eisenberg, J. F., & Wilson, D. E. (1981). Relative brain size and demographic strategies in didelphid marsupials. *The American Naturalist*, *118*(1), 1-15.

Ferreira-Cardoso, S., Araújo, R., Martins, N. E., Martins, G. G., Walsh, S., Martins, R. M. S., Kardjilov, N., Manke, I., Hilger, A., & Castanhinha, R. (2017). Floccular fossa size is not a reliable proxy of ecology and behavior in vertebrates. *Scientific Reports*, *7*(1), 1-11.

Fournier, M., Hautier, L., & Rodrigues, H. G. (2021). Evolution towards fossoriality and morphological convergence in the skull of Spalacidae and Bathyergidae (Rodentia). Journal of Mammalian Evolution, 1-15.

Freckleton, R. P., Harvey, P. H., & Pagel, M. (2002). Phylogenetic analysis and comparative data: a test and review of evidence. *The American Naturalist*, *160*(6), 712-726.

Fukushima, K., Fukushima, J., Kaneko, C. R., & Fuchs, A. F. (1999). Vertical Purkinje cells of the monkey floccular lobe: simple-spike activity during pursuit and passive whole body rotation. *Journal of neurophysiology*, *82*(2), 787-803.

Gannon, P. J., Eden, A. R., & Laitman, J. T. (1988). The subarcuate fossa and cerebellum of extant primates: Comparative study of a skull-brain interface. *American Journal of Physical Anthropology*, *77*(2), 143-164.

Gittleman, J. L. (1986). Carnivore brain size, behavioral ecology, and phylogeny. *Journal of Mammalogy*, *67*(1), 23-36.

Gittleman, J. L. (1991). Carnivore olfactory bulb size: allometry, phylogeny and ecology. *Journal of Zoology*, *225*(2), 253-272.

Glickstein, M., Gerrits, N., Kralj-Hans, I., Mercier, B., Stein, J., & Voogd, J. (1994). Visual pontocerebellar projections in the macaque. *Journal of Comparative Neurology*, *349*(1), 51-72.

Hansen, T. F. (1997). Stabilizing selection and the comparative analysis of adaptation. *Evolution*, *51*(5), 1341-1351.

Harvey, P. H., Clutton-Brock, T. H., & Mace, G. M. (1980). Brain size and ecology in small mammals and primates. *Proceedings of the National Academy of Sciences*, *77*(7), 4387-4389.

Heesy, C. P. (2004). On the relationship between orbit orientation and binocular visual field overlap in mammals. *The Anatomical Record Part A: Discoveries in Molecular, Cellular, and Evolutionary Biology: An Official Publication of the American Association of Anatomists*, *281*(1), 1104-1110.

Heesy, C. P. (2008). Ecomorphology of orbit orientation and the adaptive significance of binocular vision in primates and other mammals. *Brain, Behavior and Evolution*, *71*(1), 54-67.

Heesy, C. P. (2009). Seeing in stereo: the ecology and evolution of primate binocular vision and stereopsis. Evolutionary Anthropology: *Issues, News, and Reviews*, *18*(1), 21-35.

Hiramatsu, T., Ohki, M., Kitazawa, H., Xiong, G., Kitamura, T., Yamada, J., & Nagao, S. (2008). Role of primate cerebellar *lobulus petrosus* of paraflocculus in smooth pursuit eye movement control revealed by chemical lesion. *Neuroscience research*, *60*(3), 250-258.

Ho, L.S.T., Ane, C., Lachlan, R., Tarpinian, K., Feldman, R., Yu, Q., van der Bijl, W., Maspons, J., Vos, R. and Ho, M.L.S.T., (2016). Package 'phylolm'. *See http://cran. r-project. org/web/packages/phylolm/index. html (accessed September, 2020)*.

Hollander, J. L., Vander Wall, S. B., & Longland, W. S. (2012). Olfactory detection of caches containing wildland versus cultivated seeds by granivorous rodents. *Western North American Naturalist*, *72*(3), 339-347.

Holmes, W. G. (1991). Predator risk affects foraging behavior of pikas: observational and experimental evidence. *Animal behavior*, *42*(1), 111-119.

Howard, I. P., & Rogers, B. J. (1995). *Binocular vision and stereopsis*. Oxford University Press, USA.

Huelsenbeck, J. P., Larget, B., & Alfaro, M. E. (2004). Bayesian phylogenetic model selection using reversible jump Markov chain Monte Carlo. *Molecular biology and evolution*, *21*(6), 1123-1133.

Ilg, U. J., & Thier, P. (2008). The neural basis of smooth pursuit eye movements in the rhesus monkey brain. *Brain and cognition*, *68*(3), 229-240.

Ivins, B. L., & Smith, A. T. (1983). Responses of pikas (*Ochotona princeps*, Lagomorpha) to naturally occurring terrestrial predators. *Behavioral Ecology and Sociobiology*, *13*(4), 277-285.

Janzen, D. H. (1971). Seed predation by animals. *Annual review of ecology and systematics*, *2*(1), 465-492.

Jeffery, N., & Spoor, F. (2006). The primate subarcuate fossa and its relationship to the semicircular canals part I: prenatal growth. *Journal of human evolution*, *51*(5), 537-549.

Jeffery, N., Ryan, T. M., & Spoor, F. (2008). The primate subarcuate fossa and its relationship to the semicircular canals part II: adult interspecific variation. *Journal of human evolution*, *55*(2), 326-339.

Jerison, H. J. (1973) Evolution of the Brain and Intelligence. Academic Press

Jerison, H. J. (1979). Brain, body and encephalization in early primates. Journal of Human *Evolution*, *8*(6), 615-635.

Kaas, J. (2002). Convergences in the modular and areal organization of the forebrain of mammals: implications for the reconstruction of forebrain evolution. *Brain, behavior and evolution*, *59*(5-6), 262-272.

Kaas, J. H. (2012). The evolution of neocortex in primates. *Progress in brain research*, *195,* 91-102.

Kay, R. F., Ross, C., & Williams, B. A. (1997). Anthropoid origins. *Science*, *275*(5301), 797-804.

Kemp, A. D., & Christopher Kirk, E. (2014). Eye size and visual acuity influence vestibular anatomy in mammals. *The Anatomical Record*, *297*(4), 781-790.

Kheradmand, A., & Zee, D. S. (2011). Cerebellum and ocular motor control. *Frontiers in neurology*, *2*, 53.

Kielan-Jaworowska, Z. (1986). Brain evolution in Mesozoic mammals. *Rocky Mountain Geology*, *24*(3), 21-34.

Kirk, E. C. (2006). Visual influences on primate encephalization. *Journal of Human Evolution*, *51*(1), 76-90.

Kirk, E. C., & Kay, R. F. (2004). The evolution of high visual acuity in the Anthropoidea. In J. G. Fleagle and R. F. Kay (Eds.), Anthropoid origins (pp. 539-602). Springer, Boston, MA.

Kleinfeld, D., Ahissar, E., & Diamond, M. E. (2006). Active sensation: insights from the rodent vibrissa sensorimotor system. *Current opinion in neurobiology*, *16*(4), 435-444.

Krauzlis, R. J., & Lisberger, S. G. (1994). Simple spike responses of gaze velocity Purkinje cells in the floccular lobe of the monkey during the onset and offset of pursuit eye movements. *Journal of Neurophysiology*, *72*(4), 2045-2050.

Krubitzer, L. (1995). The organization of neocortex in mammals: are species differences really so different?. *Trends in neurosciences, 18*(9), 408-417.

Krubitzer, L., Campi, K. L., & Cooke, D. F. (2011). All rodents are not the same: a modern synthesis of cortical organization. *Brain, behavior and evolution*, *78*(1), 51-93.

Kudo, H., & Dunbar, R. I. (2001). Neocortex size and social network size in primates. *Animal Behavior*, *62*(4), 711-722.

Land, M. F. (2013). Animal vision: rats watch the sky. *Current Biology*, *23*(14), R611-R613.

Lemen, C. (1980). Relationship between relative brain size and climbing ability in *Peromyscus*. *Journal of Mammalogy*, *61*(2), 360-364.

Long, A., Bloch, J. I., & Silcox, M. T. (2015). Quantification of neocortical ratios in stem primates. American journal of physical anthropology, 157(3), 363-373.

López-Torres, S., Bertrand, O. C., Lang, M. M., Silcox, M. T., & Fostowicz-Frelik, Ł. (2020). Cranial endocast of the stem lagomorph *Megalagus* and brain structure of basal Euarchontoglires. *Proceedings of the Royal Society B*, *287*(1929), 20200665.

Lu, X., Ge, D., Xia, L., Huang, C., & Yang, Q. (2014). Geometric morphometric study of the skull shape diversification in Sciuridae (Mammalia, Rodentia). *Integrative zoology*, *9*(3), 231-245.

Mace, G. M., Harvey, P. H., & Clutton-Brock, T. H. (1981). Brain size and ecology in small mammals. *Journal of Zoology*, *193*(3), 333-354.

Macrini, T. E. (2006). The evolution of endocranial space in mammals and non-mammalian cynodonts. PhD dissertation, University of Texas, Austin.

Macrini, T. E., De Muizon, C., Cifelli, R. L., & Rowe, T. (2007a). Digital cranial endocast of Pucadelphys andinus, a Paleocene metatherian. Journal of Vertebrate Paleontology, 27(1), 99-107.

Macrini, T. E., Rougier, G. W., & Rowe, T. (2007b). Description of a cranial endocast from the fossil mammal *Vincelestes neuquenianus* (Theriiformes) and its relevance to the evolution of endocranial characters in therians. *The Anatomical Record: Advances in Integrative Anatomy and Evolutionary Biology*, *290*(7), 875-892.

Martin, R. D. (1990). Primate origins and evolution: a phylogenetic reconstruction. Chapman and Hall.

May, J. G., Keller, E. L., & Suzuki, D. A. (1988). Smooth-pursuit eye movement deficits with chemical lesions in the dorsolateral pontine nucleus of the monkey. *Journal of Neurophysiology*, *59*(3), 952-977.

McClure, T. D., & Daron, G. H. (1971). The relationship of the developing inner ear, subarcuate fossa and paraflocculus in the rat. *American Journal of Anatomy*, *130*(2), 235-249.

Meier, P. T. (1983). Relative brain size within the North American Sciuridae. *Journal of Mammalogy*, *64*(4), 642-647.

Melin, A. D., Young, H. C., Mosdossy, K. N., & Fedigan, L. M. (2014). Seasonality, extractive foraging and the evolution of primate sensorimotor intelligence. *Journal of Human Evolution*, *71*, 77-86.

Mennink, L. M., van Dijk, J. M. C., & van Dijk, P. (2020). The cerebellar (para) flocculus: A review on its auditory function and a possible role in tinnitus. *Hearing Research*, 108081.

Moncunill-Solé, B., Quintana, J., Jordana, X., Engelbrektsson, P., & Köhler, M. (2015). The weight of fossil leporids and ochotonids: body mass estimation models for the order L agomorpha. *Journal of Zoology*, *295*(4), 269-278.

Nagao, S. (1992). Different roles of flocculus and ventral paraflocculus for oculomotor control in the primate. *Neuroreport*, *3*(1), 13-16.

Nagao, S., Kitamura, T., Nakamura, N., Hiramatsu, T., & Yamada, J. (1997). Differences of the primate flocculus and ventral paraflocculus in the mossy and climbing fiber input organization. *Journal of Comparative Neurology*, *382*(4), 480-498.

Nash, L. T. (1986). Dietary, behavioral, and morphological aspects of gummivory in primates. *American journal of physical anthropology*, *29*(S7), 113-137.

Newsome, W. T., Wurtz, R. H., & Komatsu, H. (1988). Relation of cortical areas MT and MST to pursuit eye movements. II. Differentiation of retinal from extraretinal inputs. *Journal of neurophysiology*, *60*(2), 604-620.

Ni, R. J., Huang, Z. H., Luo, P. H., Ma, X. H., Li, T., & Zhou, J. N. (2018). The tree shrew cerebellum atlas: systematic nomenclature, neurochemical characterization, and afferent projections. *Journal of Comparative Neurology*, *526*(17), 2744-2775.

Nielsen, R. (2002). Mapping mutations on phylogenies. *Systematic biology*, *51*(5), 729-739.

Noda, H., & Mikami, A. (1986). Discharges of neurons in the dorsal parafloccul us of monkeys during eye movements and visual stimulation. *Journal of neurophysiology*, *56*(4), 1129-1146.

Osanai, R., Nagao, S., Kitamura, T., Kawabata, I., & Yamada, J. (1999). Differences in mossy and climbing afferent sources between flocculus and ventral and dorsal parafloccul us in the rat. *Experimental brain research*, *124*(2), 248-264.

Pagel, M. (1999). The maximum likelihood approach to reconstructing ancestral character states of discrete characters on phylogenies. *Systematic biology*, *48*(3), 612-622.

Panezai SK, Luo Y, Vibulyaseck S, Sarpong GA, Nguyen-Minh VT, Nedelescu H, Hirano S, Sugihara I. (2020). Reorganization of longitudinal compartments in the laterally protruding parafloccul us of the postnatal mouse cerebellum. *Journal of Comparative Neurology*, *528*(10), 1725-1741.

Pilleri, G., Gihr, M., & Kraus, C. (1984). Cephalization in rodents with particular reference to the Canadian beaver (Castor canadensis). *Investigations on Beavers. Brain Anatomy Institute, Berne, Switzerland*.

Powell, L. E., Isler, K., & Barton, R. A. (2017). Re-evaluating the link between brain size and behavioral ecology in primates. *Proceedings of the Royal Society B: Biological Sciences*, *284*(1865), 20171765.

R Core Team (2020). R: A Language and Environment for Statistical Computing. R Foundation for Statistical Computing, Vienna, Austria. URL http://www.R-project.org/

Rambold, H., Churchland, A., Selig, Y., Jasmin, L., & Lisberger, S. G. (2002). Partial ablations of the flocculus and ventral paraflocculus in monkeys cause linked deficits in smooth pursuit eye movements and adaptive modification of the VOR. *Journal of neurophysiology*, *87*(2), 912-924.

Rasband, W.S., ImageJ, U. S. National Institutes of Health, Bethesda, Maryland, USA, https://imagej.nih.gov/ij/, 1997-2018.

Regan, B. C., Julliot, C., Simmen, B., Viénot, F., Charles–Dominique, P., & Mollon, J. D. (2001). Fruits, foliage and the evolution of primate colour vision. *Philosophical Transactions of the Royal Society of London. Series B: Biological Sciences*, *356*(1407), 229-283.

Revell, L. J. (2012). phytools: an R package for phylogenetic comparative biology (and other things). *Methods in ecology and evolution*, *3*(2), 217-223.

Ridgway, S. H., & Hanson, A. C. (2014). Sperm whales and killer whales with the largest brains of all toothed whales show extreme differences in cerebellum. *Brain, Behavior and Evolution*, *83*(4), 266-274.

Ross, C. F. (1995). Allometric and functional influences on primate orbit orientation and the origins of the Anthropoidea. *Journal of Human Evolution*, *29*(3), 201-227.

Ross, C. F., Hall, M. I., & Heesy, C. P. (2007). Were basal primates nocturnal? Evidence from eye and orbit shape. In M. J. Ravosa and M. Dagosto (Eds.), *Primate origins: Adaptations and evolution* (pp. 233-256). Springer, Boston, MA.

Roth, V. L., & Thorington, R. W. (1982). Relative brain size among African squirrels. *Journal of Mammalogy*, *63*(1), 168-173.

Samuels, J. X., & Van Valkenburgh, B. (2008). Skeletal indicators of locomotor adaptations in living and extinct rodents. *Journal of morphology, 269*(11), 1387-1411.

Sánchez-Villagra, M. R. (2002). The cerebellar paraflocculus and the subarcuate fossa inMonodelphis domestica and other marsupial mammals—ontogeny and phylogeny of a brain-skull interaction. *Acta Theriologica*, *47*(1), 1-14.

San Martin-Flores, G., Nagendran L., Allemand R., Sargis E., and Silcox M.T. In prep. Insights into the Earliest Primates' Brains: 3-D geometric morphometric analysis of endocranial shape variation of scandentian endocasts. To be submitted to the Journal of Mammalian Evolution.

Sargis, E. J. (2002). A multivariate analysis of the postcranium of tree shrews (Scandentia, Tupaiidae) and its taxonomic implications. *Mammalia*, *66*(4), 579-598.

Sawaguchi, T., & Kudo, H. (1990). Neocortical development and social structure in primates. *Primates*, *31*(2), 283-289.

Schliep, K. P. (2011). phangorn: phylogenetic analysis in R. *Bioinformatics*, *27*(4), 592-593.

Shojaku, H., Grudt, T. J., & Barmack, N. H. (1990). Vestibular and visual signals in the ventral paraflocculus of the cerebellum in rabbits. *Neuroscience letters*, *108*(1-2), 99-104.

Spoor, F., Garland, T., Krovitz, G., Ryan, T. M., Silcox, M. T., & Walker, A. (2007). The primate semicircular canal system and locomotion. *Proceedings of the National Academy of Sciences*, *104*(26), 10808-10812.

Stafford, B. J., & Szalay, F. S. (2000). Craniodental functional morphology and taxonomy of dermopterans. Journal of mammalogy, 81(2), 360-385.

Stein, B. R. (2000) Morphology of subterranean rodents. In E. A. Lacey, J. L. Patton, & G. N. Cameron (Eds.), *Life Underground: The Biology of Subterranean Rodents* (pp. 19-61). University of Chicago Press.

Stephan, H., Frahm, H., & Baron, G. (1981). New and revised data on volumes of brain structures in insectivores and primates. *Folia primatologica*, *35*(1), 1-29.

Tan, J., Simpson, J. I., & Voogd, J. (1995). Anatomical compartments in the white matter of the rabbit flocculus. *Journal of Comparative Neurology*, *356*(1), 1-22.

Upham, N. S., Esselstyn, J. A., & Jetz, W. (2019a). Inferring the mammal tree: Species-level sets of phylogenies for questions in ecology, evolution, and conservation. *PLoS biology*, *17*(12), e3000494.

Upham, N. S., Esselstyn, J. A., & Jetz, W. (2019b). Ecological causes of uneven diversification and richness in the mammal tree of life. *bioRxiv*, 504803.

Samuels, J. X., & Van Valkenburgh, B. (2008). Skeletal indicators of locomotor adaptations in living and extinct rodents. *Journal of morphology, 269*(11), 1387-1411.

Visualization Sciences Group. 1995–2020. Avizo® 9.1.1. Konrad-ZuseZentrum fur Informationstechnik, Berlin, Germany.

Veilleux, C. C., & Kirk, E. C. (2014). Visual acuity in mammals: effects of eye size and ecology. *Brain, behavior and evolution*, *83*(1), 43-53.

Verde Arregoitia, L. D., Fisher, D. O., & Schweizer, M. (2017). Morphology captures diet and locomotor types in rodents. *Royal Society open science, 4*(1), 160957.

Volodin, I. A., Matrosova, V. A., Frey, R., Kozhevnikova, J. D., Isaeva, I. L., & Volodina, E. V. (2018). Altai pika (*Ochotona alpina*) alarm calls: individual acoustic variation and the phenomenon of call-synchronous ear folding behavior. *The Science of Nature*, *105*(7), 1-13.

Voogd, J., & Barmack, N. H. (2006). Oculomotor cerebellum. *Progress in brain research*, *151*, 231-268.

Voogd, J., Schraa-Tam, C. K., van der Geest, J. N., & De Zeeuw, C. I. (2012). Visuomotor cerebellum in human and nonhuman primates. *The Cerebellum*, *11*(2), 392-410.

Wallace, D. J., Greenberg, D. S., Sawinski, J., Rulla, S., Notaro, G., & Kerr, J. N. (2013). Rats maintain an overhead binocular field at the expense of constant fusion. *Nature*, *498*(7452), 65-69.

Walsh, S. A., Iwaniuk, A. N., Knoll, M. A., Bourdon, E., Barrett, P. M., Milner, A. C., Nudds, R.L., Abel, R.L., & Sterpaio, P. D. (2013). Avian cerebellar floccular fossa size is not a proxy for flying ability in birds. PLoS One, 8(6), e67176.

Williams, R. W., & Herrup, K. (1988). The control of neuron number. *Annual review of neuroscience*, 11(1), 423-453.

Witmer, L. M., Chatterjee, S., Franzosa, J., & Rowe, T. (2003). Neuroanatomy of flying reptiles and implications for flight, posture and behavior. *Nature*, *425*(6961), 950-953.

Wölfer, J., Amson, E., Arnold, P., Botton-Divet, L., Fabre, A. C., van Heteren, A. H., & Nyakatura, J. A. (2019). Femoral morphology of sciuromorph rodents in light of scaling and locomotor ecology. *Journal of anatomy, 234*(6), 731-747.

Xiong, G., & Nagao, S. (2002). The *lobulus petrosus* of the paraflocculus relays cortical visual inputs to the posterior interposed and lateral cerebellar nuclei: an anterograde and retrograde tracing study in the monkey. *Experimental brain research*, *147*(2), 252-263.

Xiong, G., Nagao, S., & Kitazawa, H. (2010). Mossy and climbing fiber collateral inputs in monkey cerebellar paraflocculus *lobulus petrosus* and hemispheric lobule VII and their relevance to oculomotor functions. *Neuroscience letters*, *468*(3), 282-286.

Zee, D. S., Yamazaki, A., Butler, P. H., & Gucer, G. (1981). Effects of ablation of flocculus and paraflocculus of eye movements in primate. *Journal of neurophysiology*, *46*(4), 878-899.

FIGURE LEGENDS

Figure 1. Images of *Indri indri* (AMNH 100506) endocast depicting petrosal lobules (red) and the subarcuate fossa. A) sagittal cross-section of cranium showing subarcuate fossa, B) left lateral view of endocast in semi-transparent cranium, C) right lateral view of endocast, D) ventral view of endocast, E) left lateral view of endocast; scale = 10mm.

Figure 2. Endocast of *Perodicticus potto* (MCZ 42622) showing the petrosal lobules (red) protruding through and anterior semicircular canal with semicircular canals (yellow). Endocast shown A) right lateral view of endocast, and B) ventral view of endocast; scale =10mm.

Figure 3. Endocasts for primates (purple), rodents (yellow), lagomorphs (green), scandentians (blue), and dermopterans (orange) with petrosal lobules (red). A) *Saimiri sciureus* (MCZ 30568), B) *Euoticus elegantulus* (MCZ 14658), C) *Tarsius tarsier* (USNM 200279), D) *Dryonmys nitedula* (AMNH 206584), E) *Idiurus macrotis* (AMNH 239576), F) *Rhizomys sumatrensis* (AMNH 250025), G) *Myoprocta acouchy* (AMNH 94073), H) *Lepus arcticus* (AMNH 73602), I) *Poelagus marjorita* (AMNH 118569), J) *Ochotona hyperborea* (MVZ 18367), K) *Tupaia javanica* (AMNH 101672), L) *Tupaia gracilis* (AMNH103620), M) *Cynocephalus volans* (AMNH 16697), N) *Galeopterus variegatus* (AMNH 102703); scale = 10mm.

Figure 4. Cross-section of the A) cranium and B) segmentation of endocast (blue) of *Perodicticus potto* (MCZ 42622) in the transverse plane showing the petrosal lobule (purple and red) isolation method. The right petrosal lobule shows isolation at the narrowest point of the

entrance to the subarcuate fossa and the left petrosal lobule shows isolation drawn across the two semicircular canals.

Figure 5. A) Scatter plot of $\log_{10}$ petrosal lobule volume (mm^3) plotted against $\log_{10}$ adjusted endocranial volume (mm^3) for 140 Euarchontoglires categorized by order and suborder (Primates). B) Boxplot of residuals from OLS regression of $\log_{10}$ petrosal lobule volume (mm3) plotted against $\log_{10}$ adjusted endocranial volume (mm^3) categorized by order and suborder (Primates). C) Scatter plot of $\log_{10}$ petrosal lobule mass (g) plotted against $\log_{10}$ adjusted body mass (g) for 140 Euarchontoglires categorized by order and suborder (Primates). D) Boxplot of residuals from OLS regression of $\log_{10}$ petrosal lobule mass (g) plotted against $\log_{10}$ adjusted body mass (g) categorized by order and suborder (Primates).

Figure 6. Ancestral character state reconstruction of lobule size (as determined from subarcuate fossa size) using residuals from ordinary least squares (OLS) regression analyses for lobule volume/mass plotted against A) AEV and B) ABM. Scale reflects residual values. Fossorial taxa highlighted in grey. (Phylogenetic tree produced using maximum clade credibility for this sample of 140 euarchontoglirans, based on 10,000 fossil calibrated node-dated credible trees).

Figure 7. Boxplot of residuals from PGLS regression of $\log_{10}$ petrosal lobule volume (mm^3) plotted against $\log_{10}$ adjusted endocranial volume (mm^3) and $\log_{10}$ petrosal lobule mass (g) plotted against $\log_{10}$ adjusted body mass (g) for 137 Euarchontoglires categorized by locomotor behavior (A,B), diet (C,D), and activity pattern (E,F).

TABLE LEGENDS

Table 1. List of species and associated petrosal lobule volumes (PLV), total endocranial volumes (ECV), petrosal lobule percent of endocranial volume (%PLV), body mass estimates (BM), and ecological categories for locomotor behavior, activity pattern, and diet.

Foot Note: Museum Abbreviations: National Council of Science Museums (NCSM), Museum of Vertebrate Zoology (MVZ), American Museum of Natural History (AMNH), Smithsonian National Museum of Natural History (USNM), University Museum of Zoology, Cambridge (UMZC), Florida Museum of Natural History (UF), Digital Preservation Coalition (DPC), Museum of Comparative Zoology (MCZ), Field Museum of Natural History (FMNH).

Table 2. Regression equations and measurements used to estimate body masses by taxonomic group with sources. Log 10 applied to all raw data.

Table 3. Regression statistics from petrosal lobule analyses of $\log_{10}$ petrosal lobule volume (mm^3) plotted against $\log_{10}$ adjusted endocranial volume (mm^3) (PLV~AEV) and $\log_{10}$ petrosal lobule mass (g) plotted against $\log_{10}$ adjusted body mass (g) (PLM~ABM) using PGLS (Pagle's λ) and Ordinary Least Squares (OLS) linear modelling for Euarchontoglires (n = 140), Rodentia (n = 71), and Primates (n = 38) separately.

Table 4a. Results from ANOVA of residuals from ordinary least squares (OLS) regression of $\log_{10}$ petrosal lobule volume (mm^3) plotted against $\log_{10}$ adjusted endocranial volume (mm^3)

(PLV~AEV) and $\log_{10}$ petrosal lobule mass (g) plotted against $\log_{10}$ adjusted body mass (g) (PLM~ABM) by Order.

Table 4b. Results of post hoc tests based on analysis of variance of residuals from ordinary least squares (OLS) regression of $\log_{10}$ petrosal lobule volume (mm^3) plotted against $\log_{10}$ adjusted endocranial volume (mm^3) (PLV~AEV) and $\log_{10}$ petrosal lobule mass (g) plotted against $\log_{10}$ adjusted body mass (g) (PLM~ABM) by Order.

Table 5a. Results from ANOVA of residuals from ordinary least squares (OLS) regression of $\log_{10}$ petrosal lobule volume (mm^3) plotted against $\log_{10}$ adjusted endocranial volume (mm^3) (PLV~AEV) and $\log_{10}$ petrosal lobule mass (g) plotted against $\log_{10}$ adjusted body mass (g) (PLM~ABM) by Order and Suborder for Primates (Haplorhini and Strepsirrhini).

Table 5b. Results of post hoc tests based on analysis of variance (ANOVA) of residuals from ordinary least squares (OLS) regression of $\log_{10}$ petrosal lobule volume (mm^3) plotted against $\log_{10}$ adjusted endocranial volume (mm^3) (PLV~AEV) and $\log_{10}$ petrosal lobule mass (g) plotted against $\log_{10}$ adjusted body mass (g) (PLM~ABM) by Order and Suborder for Primates (Haplorhini and Strepsirrhini).

Table 6a. Results of phylogenetic analysis of variance (pANOVA) of residuals from PGLS regression of $\log_{10}$ petrosal lobule volume (mm^3) plotted against $\log_{10}$ adjusted endocranial volume (mm^3) (PLV~AEV) and $\log_{10}$ petrosal lobule mass (g) plotted against $\log_{10}$ adjusted body

mass (g) (PLM~ABM) by primary ecological categories for locomotor behavior, activity pattern, and diet in Euarchontoglires.

Table 6b. Results of post hoc tests based on phylogenetic analysis of variance (pANOVA) of residuals from PGLS regression of log_{10} petrosal lobule mass (g) plotted against log_{10} adjusted body mass (g) (PLM~ABM) for locomotor behavior in Euarchontoglires.

Foot Note: Arboreal (Ar), Cursorial (Cu), Fossorial (Fo.), Gliding (Gl), Saltatorial (Sl), Scansorial (Sc), Semiaquatic (Sa), Slow Arboreal (SAr) Terrestrial (Tr).

Table 7. Results of phylogenetic analysis of variance (pANOVA) of residuals from PGLS regression of log_{10} petrosal lobule volume (mm^3) plotted against log_{10} adjusted endocranial volume (mm^3) (PLV~AEV) and log_{10} petrosal lobule mass (g) plotted against log_{10} adjusted body mass (g) (PLM~ABM) by primary ecological categories for locomotor behavior, activity pattern, and diet in Rodents.

Table 8. Results of phylogenetic analysis of variance (pANOVA) of residuals from PGLS regression of log_{10} petrosal lobule volume (mm^3) plotted against log_{10} adjusted endocranial volume (mm^3) (PLV~AEV) and log_{10} petrosal lobule mass (g) plotted against log_{10} adjusted body mass (g) (PLM~ABM) by primary ecological categories for locomotor behavior, activity pattern, and diet in Primates.

Table 9a. Comparisons of evolutionary model fit for petrosal lobules volume based on residuals of OLS regression of log_{10} petrosal lobule volume (mm^3) plotted against log_{10} adjusted endocranial volume (mm^3).

Table 9b. Comparisons of evolutionary model fit for petrosal lobules volume based on residuals of OLS regression of and log_{10} petrosal lobule mass (g) plotted against log_{10} adjusted body mass (g).

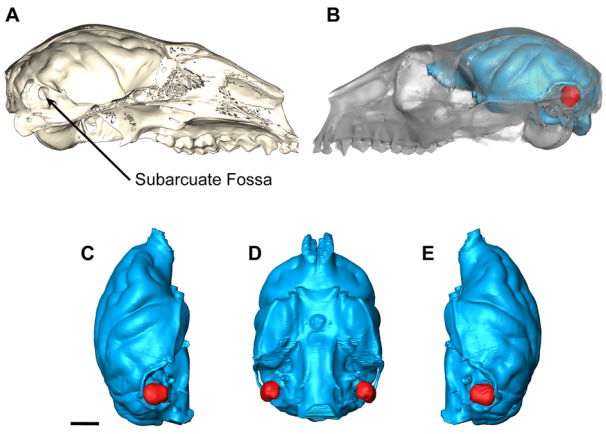

AR_24929_Figure 1.R2.tif

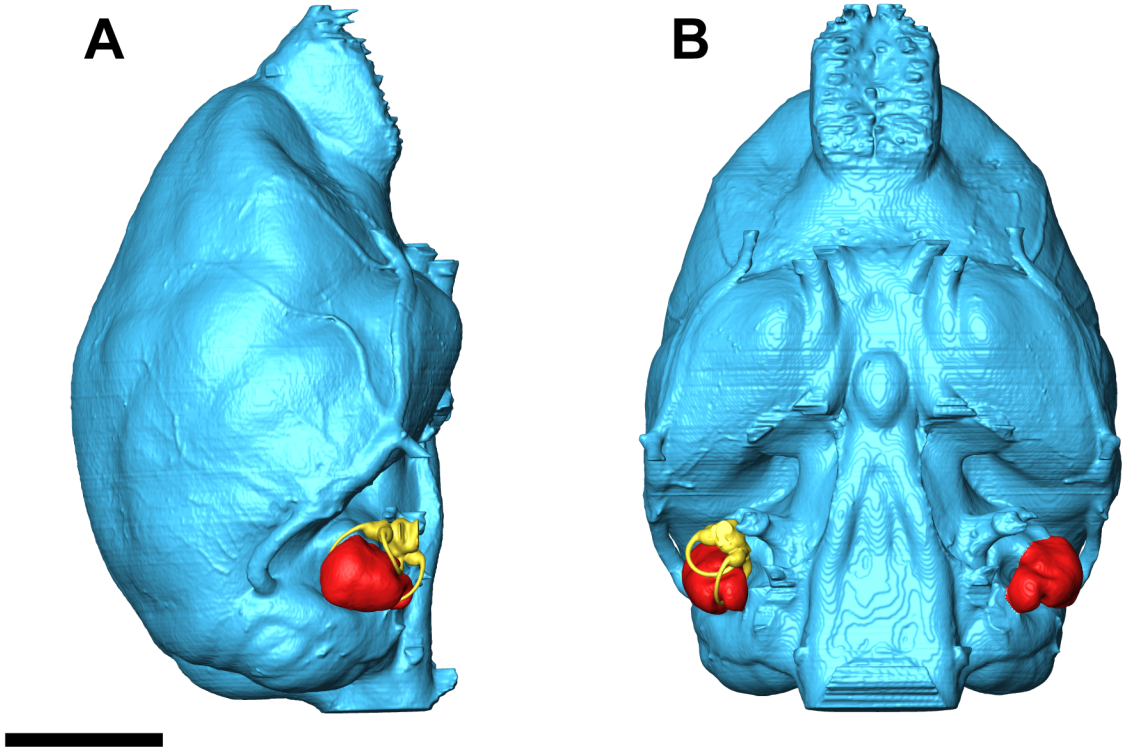

AR_24929_Figure 2.tif

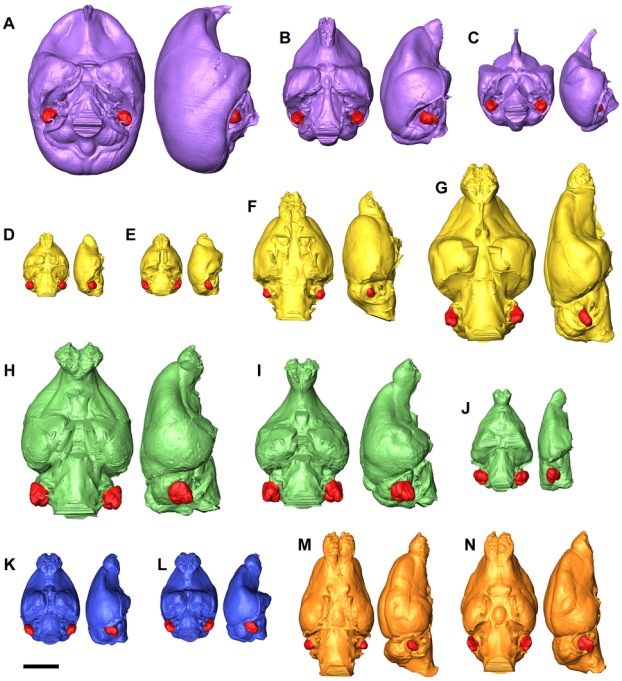

AR_24929_Figure 3.R2.tif

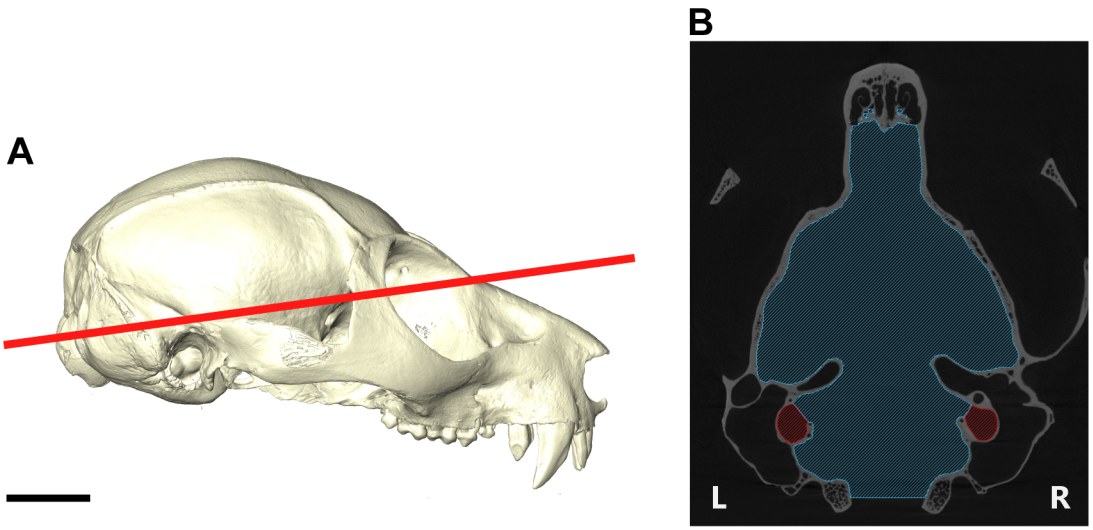

AR_24929_Figure 4.tif

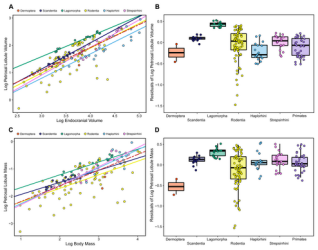

AR_24929_Figure 5.R2.tif

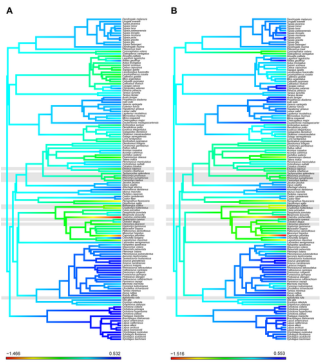

AR_24929_Figure_6.R2.tif

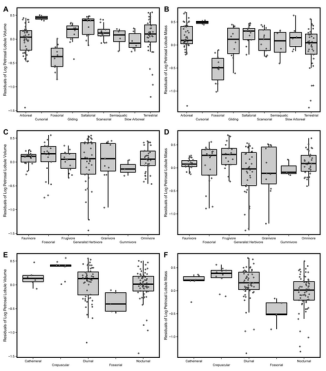

AR_24929_Figure 7.R2.tif

Table 1. List of species and associated petrosal lobule volumes (PLV), total endocranial volumes (ECV), petrosal lobule percent of endocranial volume (%PLV), body mass estimates (BM), and ecological categories for locomotor behaviour, activity pattern, and diet.

Order	Species	Catalogue#	ECV(mm^3)	PLV(mm^3)	% PLV	BM(g)	Locomotion	Activity Pattern	Diet
Lagomorpha	*Sylvilagus bachmani*	*MVZ 228957*	5967.82	126.86	2.13	973.33	Saltatorial	Crepuscular	Folivore
	Sylvilagus audubonii	*MVZ 43914*	7688.30	158.17	2.06	715.40	Saltatorial	Crepuscular	Generalist Herbivore
	Sylvilagus floridanus	*NCSM 8490*	8456.42	199.27	2.36	1741.87	Saltatorial	Crepuscular	Generalist Herbivore
	Oryctolagus cuniculus	*AMNH 34816*	9156.09	207.03	2.26	1796.07	Saltatorial	Nocturnal	Folivore
	Lepus townsendii	*MVZ 20773*	13923.30	303.30	2.18	2265.02	Saltatorial	Nocturnal	Generalist Herbivore
	Lepus arcticus	*AMNH 42139*	15679.80	270.10	1.72	4003.10	Saltatorial	Crepuscular	Generalist Herbivore
	Lepus alleni	*MVZ 76201*	15945.70	275.22	1.73	2183.01	Cursorial	Crepuscular	Generalist Herbivore
	Lepus californicus	*NCSM 8305*	14218.60	325.40	2.29	1955.70	Cursorial	Nocturnal	Generalist Herbivore
	Lepus americanus	*AMNH97648*	10020.40	201.00	2.01	998.68	Saltatorial	Nocturnal	Generalist Herbivore
	Brachylagus idahoensis	*AMNH 92869*	4992.15	153.04	3.07	339.56	Terrestrial	Crepuscular	Folivore
	Poelagus marjorita	*AMNH 51052*	11597.13	210.83	1.82	2480.24	Saltatorial	Nocturnal	Generalist Herbivore
	Ochotona pallasi	*AMNH 59712*	2078.92	59.32	2.85	223.85	Terrestrial	Cathemeral	Generalist Herbivore
	Ochotona hyperborea	*MVZ 183687*	1992.21	57.11	2.87	118.87	Terrestrial	Diurnal	Generalist Herbivore
	Ochotona princeps	*AMNH 120698*	2195.74	74.74	3.40	202.92	Terrestrial	Diurnal	Generalist Herbivore
	Ochotona collaris	*MVZ 183686*	2412.48	76.33	3.16	128.78	Terrestrial	Diurnal	Generalist Herbivore
Rodentia	*Graphiurus platyops*	*AMNH 88170*	951.69	8.89	0.93	42.61	Scansorial	Nocturnal	Omnivore
	Dryomys nitedula	*AMNH 206584*	940.03	14.30	1.52	29.99	Arboreal	Nocturnal	Faunivore
	Glis glis	*AMNH 160904*	1895.41	29.79	1.57	105.92	Arboreal	Nocturnal	Generalist Herbivore
	Aplodontia rufa	*AMNH 42389*	7892.50	64.41	0.82	1470.15	Fossorial	Nocturnal	Generalist Herbivore
	Ratufa affinis	*USNM 488104*	12313.70	233.00	1.89	1070.19	Arboreal	Diurnal	Omnivore
	Xerus rutilus	*AMNH 179092*	6001.71	113.01	1.88	352.65	Terrestrial	Diurnal	Granivore
	Paraxerus cepapi	*USNM 367956*	3053.30	44.66	1.46	137.67	Scansorial	Cathemeral	Omnivore
	Heliosciurus rufobrachium	*USNM 378091*	6076.64	113.61	1.87	353.72	Arboreal	Diurnal	Omnivore
	Protoxerus stangeri	*USNM 435027*	6076.64	113.61	1.87	764.37	Arboreal	Diurnal	Omnivore
	Funisciurus pyrropus	*USNM 435043*	4554.13	99.54	2.19	300.09	Scansorial	Crepuscular	Omnivore
	Tamias minimus	*USNM 298500*	1521.38	34.80	2.29	36.94	Scansorial	Diurnal	Omnivore
	Urocitellus richardsonii	*AMNH 146619*	3157.99	55.33	1.75	245.78	Terrestrial	Diurnal	Generalist Herbivore
	Cynomys ludovicianus	*AMNH114522*	7220.30	70.97	0.98	938.70	Terrestrial	Diurnal	Generalist Herbivore
	Marmota marmota	*AMNH 15062*	15195.80	127.40	0.84	4546.97	Terrestrial	Diurnal	Generalist Herbivore
	Dremomys rufigenis	*USNM 488602*	5866.09	125.71	2.14	416.93	Scansorial	Diurnal	Omnivore
	Callosciurus caniceps	*USNM 294865*	7007.94	123.91	1.77	435.77	Arboreal	Diurnal	Frugivore
	Rhinosciurus laticaudatus	*USNM 488511*	4383.60	97.36	2.22	505.54	Terrestrial	Diurnal	Omnivore
	Lariscus insignis	*USNM 488570*	4878.57	113.00	2.32	323.56	Terrestrial	Diurnal	Omnivore
	Sciurus carolinensis	*AMNH 258346*	8052.59	163.26	2.03	590.38	Arboreal	Crepuscular	Granivore
	Sciurus granatensis	*USNM 441999*	6323.66	131.63	2.08	335.80	Arboreal	Diurnal	Granivore

Table 1. Continued.

Order	Species	Catalogue#	ECV(mm^3)	PLV(mm^3)	% PLV	BM(g)	Locomotion	Activity Pattern	Diet
	Tamiasciurus hudsonicus	*USNM 549146*	5146.70	120.02	2.33	255.72	Arboreal	Diurnal	Granivore
	Aeromys tephromelas	*USNM 481190*	11461.50	166.10	1.45	901.19	Gliding	Nocturnal	Folivore
	Pteromyscus pulverulentus	*UMNH 481178*	3621.04	49.50	1.37	194.77	Gliding	Nocturnal	Frugivore
	Pteromys volans	*USNM 172622*	2330.80	37.53	1.61	1070.19	Gliding	Nocturnal	Folivore
	Petaurista petaurista	*UMNH 589079*	12317.70	199.90	1.62	1092.47	Gliding	Nocturnal	Folivore
	Glaucomys volans	*AMNH 240290*	2010.43	33.73	1.68	63.76	Gliding	Nocturnal	Omnivore
	Hylopetes spadiceus	*UNMH 488639*	2120.74	17.93	0.85	83.95	Gliding	Nocturnal	Generalist Herbivore
	Laonastes aenigmamus	*HLKY213*	5578.76	65.68	1.18	885.09	Terrestrial	Nocturnal	Generalist Herbivore
	Lagostomus maximus	*AMNH 41523*	13326.70	17.60	0.13	4155.91	Terrestrial	Nocturnal	Folivore
	Chinchilla lanigera	*AMNH 180038*	5602.34	100.19	1.79	725.02	Terrestrial	Nocturnal	Folivore
	Capromys pilorides	*UMZC E 3371*	13731.90	6.20	0.05	4674.27	Terrestrial	Diurnal	Generalist Herbivore
	Mesomys hispidus	*AMNH 80434*	2897.73	29.22	1.01	191.53	Arboreal	Nocturnal	Omnivore
	Pattonomys semivillosus	*AMNH 96763*	5625.19	40.02	0.71	792.95	Arboreal	Nocturnal	Frugivore
	Myocastor coypus	*AMNH 93320*	18039.60	70.70	0.39	7569.19	Semi-aquatic	Nocturnal	Generalist Herbivore
	Hoplomys gymnurus	*AMNH 29548*	4928.85	29.41	0.60	689.41	Terrestrial	Nocturnal	Frugivore
	Ctenomys pearsoni	*AMNH 206517*	2421.58	4.65	0.19	196.67	Fossorial	Diurnal	Folivore
	Octodon degus	*AMNH 242477*	2135.45	22.68	1.06	104.07	Terrestrial	Diurnal	Generalist Herbivore
	Spalacopus cyanus	*AMNH 33277*	1665.01	7.85	0.47	99.41	Fossorial	Diurnal	Generalist Herbivore
	Coendou prehensilis	*UF 14899*	22473.00	5.60	0.02	3113.37	Arboreal	Nocturnal	Generalist Herbivore
	Myoprocta acouchy	*AMNH 94073*	12932.70	73.00	0.56	2189.32	Terrestrial	Diurnal	Granivore
	Dasyprocta punctata	*AMNH 14179*	21968.30	168.80	0.77	4772.96	Terrestrial	Diurnal	Frugivore
	Cavia porcellus	*HACB CP3*	5729.85	25.91	0.45	1147.76	Terrestrial	Nocturnal	Granivore
	Cryptomys hottentotus	*AMNH 219061*	1284.96	1.95	0.15	71.90	Fossorial	Nocturnal	Generalist Herbivore
	Bathyergus suillus	*AMNH 168285*	3826.55	8.91	0.23	776.39	Fossorial	Fossorial	Generalist Herbivore
	Dipodomys agilis	*AMNH 68717*	1239.04	12.24	0.99	68.92	Saltatorial	Nocturnal	Generalist Herbivore
	Perognathus flavescens	*AMNH 104526*	340.53	0.49	0.14	9.77	Terrestrial	Nocturnal	Granivore
	Castor fiber	*AMNH 244285*	44663.90	390.10	0.87	11561.39	Semi-aquatic	Nocturnal	Folivore
	Castor canadensis	*AMNH 258793*	42745.50	427.10	1.00	10347.60	Semi-aquatic	Nocturnal	Folivore
	Pedetes capensis	*AMNH 168880*	19544.40	100.60	0.51	2627.64	Saltatorial	Nocturnal	Folivore
	Idiurus macrotis	*AMNH 239579*	926.66	12.90	1.39	20.61	Gliding	Nocturnal	Folivore
	Anomalurus derbianus	*AMNH 116551*	6150.99	106.35	1.73	332.45	Gliding	Nocturnal	Folivore
	Allactaga sibirica	*AMNH 58863*	2040.04	35.56	1.74	86.36	Saltatorial	Nocturnal	Faunivore
	Dipus sagitta	*UMZC E.3165*	2645.07	29.41	1.11	90.75	Saltatorial	Nocturnal	Granivore
	Jaculus jaculus	*AMNH 184987*	1803.63	22.43	1.24	54.06	Saltatorial	Nocturnal	Generalist Herbivore
	Cannomys badius	*UMZC E 2850*	2771.32	17.67	0.64	199.46	Fossorial	Fossorial	Generalist Herbivore
	Rhizomys pruinosus	*AMNH 112998*	6862.46	43.20	0.63	841.66	Fossorial	Fossorial	Generalist Herbivore
	Rhizomys sumatrensis	*AMNH 250025*	5284.54	12.45	0.24	343.36	Fossorial	Fossorial	Generalist Herbivore

Table 1. Continued.

Order	Species	Catalogue#	ECV(mm^3)	PLV(mm^3)	% PLV	BM(g)	Locomotion	Activity Pattern	Diet
	Tachyoryctes splendens	*AMNH 269633*	2493.87	12.95	0.52	174.29	Fossorial	Nocturnal	Generalist Herbivore
	Ondatra zibethicus	*AMNH 270062*	6266.19	53.33	0.85	845.26	Semi-aquatic	Crepuscular	Generalist Herbivore
	Ellobius talpinus	*AMNH 97838*	984.56	4.28	0.43	32.44	Fossorial	Fossorial	Generalist Herbivore
	Cricetus cricetus	*AMNH 176484*	1993.82	22.32	1.12	141.56	Terrestrial	Nocturnal	Omnivore
	Ochrotomys nuttalli	*AMNH 215371*	658.86	8.96	1.36	22.82	Scansorial	Crepuscular	Granivore
	Peromyscus maniculatus	*AMNH 140807*	646.31	10.06	1.56	23.45	Scansorial	Nocturnal	Omnivore
	Tatera indica	*AMNH 250026*	1947.40	11.18	0.57	142.78	Terrestrial	Nocturnal	Omnivore
	Psammomys obesus	*AMNH 203215*	1430.40	3.53	0.25	130.76	Terrestrial	Diurnal	Generalist Herbivore
	Gerbillus watersi	*UMZC E.1971*	493.05	3.25	0.66	16.80	Terrestrial	Nocturnal	Granivore
	Acomys cahirinus	*AMNH 241326*	686.18	8.52	1.24	30.11	Terrestrial	Nocturnal	Omnivore
	Acomys russatus	*AMNH 238096*	841.77	11.88	1.41	42.33	Terrestrial	Diurnal	Omnivore
	Rattus rattus	*AMNH 275420*	1980.85	16.32	0.82	136.35	Scansorial	Nocturnal	Omnivore
	Cricetomys gambianus	*UMZC E 2261*	6599.58	48.69	0.74	1308.99	Terrestrial	Nocturnal	Omnivore
	Dendromus insignis	*AMNH 181028*	437.36	4.51	1.03	9.77	Scansorial	Cathemeral	Granivore
Primates	*Nycticebus pygmaeus*	*MCZ 6035*	7125.36	29.72	0.42	356.99	Arboreal	Nocturnal	Gummivore
	Loris tardigradus	*BAA 0006*	6411.77	33.91	0.53	343.92	Slow Arborealist	Nocturnal	Faunivore
	Galago senegalensis	*MCZ 44134*	4215.87	33.60	0.80	188.72	Arboreal	Nocturnal	Omnivore
	Otolemur crassicaudatus	*AMNH 80800*	13277.00	69.10	0.52	1628.34	Arboreal	Nocturnal	Gummivore
	Galagoides demidovii	*AMNH 50984*	2401.69	21.82	0.91	72.68	Arboreal	Nocturnal	Faunivore
	Euoticus elegantulus	*MCZ 14658*	6797.01	60.82	0.89	312.53	Arboreal	Nocturnal	Gummivore
	Perodicticus potto	*MCZ 42622*	15389.30	101.30	0.66	972.19	Slow Arborealist	Nocturnal	Omnivore
	Arctocebus aureus	*YPM 014401*	8291.01	36.06	0.43	486.75	Slow Arborealist	Nocturnal	Faunivore
	Daubentonia madagascariensis	*AMNH 100632*	42309.70	435.90	1.03	2166.51	Slow Arborealist	Nocturnal	Omnivore
	Cheirogaleus major	*AMNH 100640*	6342.91	71.28	1.12	507.39	Arboreal	Nocturnal	Omnivore
	Mirza coquereli	*DPC 0137*	6576.32	50.86	0.77	345.21	Arboreal	Nocturnal	Omnivore
	Microcebus murinus	*MCZ 45125*	1395.93	18.00	1.29	61.47	Arboreal	Nocturnal	Omnivore
	Lepilemur mustelinus	*AMNH 170558*	7603.27	88.52	1.16	375.63	Slow Arborealist	Nocturnal	Folivore
	Lemur catta	*MCZ 44903*	24563.00	205.70	0.84	2066.28	Scansorial	Cathemeral	Frugivore
	Hapalemur griseus	*MCZ 44911*	13700.70	146.30	1.07	884.88	Arboreal	Cathemeral	Folivore
	Eulemur fulvus	*MCZ 44896*	25991.00	193.50	0.74	3132.42	Arboreal	Cathemeral	Frugivore
	Varecia variegata	*MCZ 44905*	34771.40	324.10	0.93	5946.82	Arboreal	Diurnal	Frugivore
	Indri indri	*AMNH 100506*	37127.60	367.20	0.99	5039.75	Arboreal	Diurnal	Folivore
	Propithecus diadema	*MCZ 5016*	38825.10	439.00	1.13	2869.45	Arboreal	Diurnal	Frugivore
	Avahi laniger	*MCZ32503*	9308.34	106.56	1.14	341.09	Arboreal	Nocturnal	Folivore
	Tarsius tarsier	*USNM 200279*	2907.57	25.39	0.87	98.60	Arboreal	Nocturnal	Faunivore
	Tarsius syrichta	*USNM282761*	4121.58	33.56	0.81	139.31	Arboreal	Nocturnal	Faunivore
	Pithecia pithecia	*MCZ 31061*	29878.00	221.50	0.74	1669.48	Arboreal	Diurnal	Frugivore

Table 1. Continued.

Order	Species	Catalogue#	ECV(mm^3)	PLV(mm^3)	% PLV	BM(g)	Locomotion	Activity Pattern	Diet
	Chiropotes satanas	*MCZ 6028*	55600.80	492.50	0.89	2326.18	Arboreal	Diurnal	Frugivore
	Cacajao calvus	*MCZ 1957*	68491.80	394.00	0.58	3532.10	Arboreal	Diurnal	Frugivore
	Callicebus moloch	*MCZ 26922*	18810.30	61.10	0.32	802.79	Arboreal	Diurnal	Frugivore
	Cebuella pygmaea	*USNM 337324*	3679.19	16.86	0.46	47.44	Arboreal	Diurnal	Omnivore
	Mico argentatus	*MCZ 30579*	7930.20	39.44	0.50	191.33	Arboreal	Diurnal	Omnivore
	Callimico goeldii	*AMNH 98367*	12866.10	41.90	0.33	285.30	Arboreal	Diurnal	Omnivore
	Leontopithecus rosalia	*AMNH 235274*	11863.20	30.80	0.26	493.02	Arboreal	Diurnal	Omnivore
	Leontocebus fuscicollis	*AMNH 74042*	9421.15	41.77	0.44	255.63	Arboreal	Diurnal	Frugivore
	Sapajus apella	*MCZ 41090*	68811.50	151.70	0.22	3694.71	Arboreal	Diurnal	Omnivore
	Cebus capucinus	*MCZ 34326*	68488.50	203.00	0.30	4366.25	Arboreal	Diurnal	Omnivore
	Saimiri sciureus	*MCZ 30568*	20353.50	71.00	0.35	581.02	Arboreal	Diurnal	Omnivore
	Aotus trivirgatus	*MCZ 19802*	15265.70	80.20	0.53	684.15	Slow Arborealist	Nocturnal	Frugivore
	Ateles geoffroyi	*MCZ BOM-5346*	106133.00	893.00	0.84	7214.74	Arboreal	Diurnal	Frugivore
	Lagothrix lagotricha	*USNM 194342*	101254.00	290.00	0.29	5227.72	Arboreal	Diurnal	Frugivore
	Alouatta palliata	*MCZ 6001*	47553.30	97.70	0.21	4641.89	Arboreal	Diurnal	Folivore
Dermoptera	*Galeopterus variegatus*	*AMNH 102703*	5897.58	49.40	0.84	1100.00	Gliding	Nocturnal	Folivore
	Cynocephalus volans	*AMNH 16697*	5869.34	18.71	0.32	1500.00	Gliding	Nocturnal	Folivore
Scandentia	*Ptilocercus lowii*	*USNM 481103*	1645.13	16.72	1.02	45.30	Arboreal	Nocturnal	Faunivore
	Dendrogale murina	*FMNH 46629*	1405.24	20.69	1.47	45.00	Arboreal	Diurnal	Faunivore
	Tupaia belangeri	*USNM 320655*	3854.83	48.23	1.25	145.40	Terrestrial	Diurnal	Faunivore
	Tupaia glis	*USNM 311311*	3444.91	40.03	1.16	152.20	Scansorial	Diurnal	Faunivore
	Tupaia gracilis	*AMNH 103620*	2215.67	36.38	1.64	67.10	Terrestrial	Diurnal	Faunivore
	Tupaia picta	*UMZC E4063A*	3336.63	43.38	1.30	34.30	Scansorial	Diurnal	Faunivore
	Tupaia montana	*FMNH 108831*	2810.09	37.26	1.33	126.00	Terrestrial	Diurnal	Faunivore
	Tupaia dorsalis	*AMNH 1103892*	2465.00	30.21	1.23	26.50	Terrestrial	Diurnal	Faunivore
	Tupaia palawanensis	*FMNH 62948*	2950.49	33.56	1.14	138.50	Terrestrial	Diurnal	Faunivore
	Tupaia tana	*AMNH 102829*	3712.24	55.39	1.49	205.30	Terrestrial	Diurnal	Faunivore
	Tupaia minor	*AMNH 103906*	1755.63	21.25	1.21	54.40	Arboreal	Diurnal	Faunivore
	Tupaia javanica	*AMNH 101672*	2289.09	32.52	1.42	87.80	Scansorial	Diurnal	Faunivore
	Urogale everetti	*FMNH 61419*	4530.12	53.54	1.18	224.00	Terrestrial	Diurnal	Omnivore
	Dendrogale melanura	*FMNH 108854*	1480.2	20.08	1.36	49.5	Terrestrial	Diurnal	Faunivore

Museum Abbreviations: National Council of Science Museums (NCSM), Museum of Vertebrate Zoology (MVZ), American Museum of Natural History (AMNH), Smithsonian National Museum of Natural History (USNM), University Museum of Zoology, Cambridge (UMZC), Florida Museum of Natural History (UF), Digital Preservation Coalition (DPC), Museum of Comparative Zoology (MCZ), Field Museum of Natural History (FMNH).

Table 2. Regression equations and measurements used to estimate body masses by taxonomic group with sources. Log 10 applied to all raw data.

Source	Taxon	Measurement (mm)	Unit	slope	y-int	*p*	r^2
Silcox et al. (2009)	Prosimian	prosthion inion length	kg	3.79	-6.92	<0.0001	0.93
Martin (1990)	Simian	maximal skull length	g	3.89	-4.09	-	0.98
Bertrand et al. (2015)	Rodentia	maximal skull length	g	3.95	-4.23	-	0.96
Moncunill-Solé et al. (2015)	Lagomorpha	maximal occipital condyle width	g	4.09	−1.526	0.000	0.96

Table 3. Regression statistics from petrosal lobule analyses of log_{10} petrosal lobule volume (mm^3) plotted against log_{10} adjusted endocranial volume (mm^3) (PLV~AEV) and log_{10} petrosal lobule mass (g) plotted against log_{10} adjusted body mass (g) (PLM~ABM) using PGLS (Pagle's λ) and Ordinary Least Squares (OLS) linear modelling for Euarchontoglires (n = 140), Rodentia (n = 71), and Primates (n = 38) separately.

	Data	Models	Slope	Intercept b	r^2	sig. (*p*)	λ	AIC	LogLik
Euarchontoglires	*PLV~AEV*	*Pagel's λ*	0.845	-1.494	0.600	0.000	0.966	3.137	2.432
		OLS	0.842	-1.450	0.615	0.001	NA	NA	NA
	PLM~ABM	*Pagel's λ*	0.466	-2.546	0.482	0.000	0.949	40.760	-16.380
		OLS	0.575	-2.776	0.524	0.001	NA	NA	NA
Rodentia	*PLV~AEV*	*Pagel's λ*	0.835	-1.524	0.524	0.000	0.777	47.060	-19.530
		OLS	0.907	-1.734	0.545	0.001	NA	NA	NA
	PLM~ABM	*Pagel's λ*	0.458	-2.704	0.424	0.000	0.861	59.450	-25.720
		OLS	0.497	-2.741	0.400	0.001	NA	NA	NA
Primates	*PLV~AEV*	*Pagel's λ*	0.920	-1.843	0.829	0.000	0.761	-20.820	14.410
		OLS	0.855	-1.603	0.781	0.001	NA	NA	NA
	PLM~ABM	*Pagel's λ*	0.661	-2.956	0.792	0.000	0.15	-5.619	6.809
		OLS	0.673	-2.994	0.801	0.001	NA	NA	NA

Table 4a. Results from ANOVA of residuals from ordinary least squares (OLS) regression of log_{10} petrosal lobule volume (mm^3) plotted against log_{10} adjusted endocranial volume (mm^3) (PLV~AEV) and log_{10} petrosal lobule mass (g) plotted against log_{10} adjusted body mass (g) (PLM~ABM) by Order.

Data	Df	SS	Residual SS	R^2	F	Z	sig. (*p*)
PLV~AEV	4	3.616	12.765	0.221	9.559	3.050	0.001
PLM~ABM	4	3.681	16.534	0.182	7.515	2.738	0.002

Table 4b. Results of post hoc tests based on analysis of variance of residuals from ordinary least squares (OLS) regression of log_{10} petrosal lobule volume (mm^3) plotted against log_{10} adjusted endocranial volume (mm^3) (PLV~AEV) and log_{10} petrosal lobule mass (g) plotted against log_{10} adjusted body mass (g) (PLM~ABM) by Order.

Data	*Order*	Dermoptera	Lagomorpha	Primates	Rodentia	Scandentia
PLV~AEV	Dermoptera	-	**0.021**	0.557	0.433	0.184
	Lagomorpha	**0.021**	-	**0.001**	**0.001**	**0.014**
	Primates	0.557	**0.001**	-	0.482	0.059
	Rodentia	0.433	**0.001**	0.482	-	0.133
	Scandentia	0.184	**0.014**	0.059	0.133	-

Data	*Order*	Dermoptera	Lagomorpha	Primates	Rodentia	Scandentia
PLM~ABM	Dermoptera	-	**0.010**	**0.042**	0.128	**0.039**
	Lagomorpha	**0.010**	-	0.064	**0.001**	0.202
	Primates	**0.042**	0.064	-	**0.007**	0.825
	Rodentia	0.128	**0.001**	**0.007**	-	**0.031**
	Scandentia	**0.039**	0.202	0.825	**0.031**	-

Table 5a. Results from ANOVA of residuals from ordinary least squares (OLS) regression of log_{10} petrosal lobule volume (mm^3) plotted against log_{10} adjusted endocranial volume (mm^3) (PLV~AEV) and log_{10} petrosal lobule mass (g) plotted against log_{10} adjusted body mass (g) (PLM~ABM) by Order and Suborder for Primates (Haplorhini and Strepsirrhini).

Data	Df	SS	Residual SS	R^2	F	Z	sig. (*p*)
PLV~AEV	5	4.096	12.284	0.250	8.937	3.296	0.001
PLM~ABM	5	3.688	16.528	0.182	5.980	2.703	0.002

Table 5b. Results of post hoc tests based on analysis of variance (ANOVA) of residuals from ordinary least squares (OLS) regression of log_{10} petrosal lobule volume (mm^3) plotted against log_{10} adjusted endocranial volume (mm^3) (PLV~AEV) and log_{10} petrosal lobule mass (g) plotted against log_{10} adjusted body mass (g) (PLM~ABM) by Order and Suborder for Primates (Haplorhini and Strepsirrhini).

Data	Order	Dermoptera	Haplorrhini	Lagomorpha	Rodentia	Scandentia	Strepsirrhini
PLV~AEV	Dermoptera	-	0.927	**0.021**	0.433	0.184	0.313
	Haplorrhini	0.927	-	**0.001**	0.060	**0.009**	**0.043**
	Lagomorpha	**0.021**	**0.001**		**0.001**	**0.014**	**0.001**
	Rodentia	0.433	0.060	**0.001**	-	0.133	0.504
	Scandentia	0.184	**0.009**	**0.014**	0.133	-	0.429
	Strepsirrhini	0.313	**0.043**	**0.001**	0.504	0.429	-
Data	Order	Dermoptera	Haplorrhini	Lagomorpha	Rodentia	Scandentia	Strepsirrhini
PLM~ABM	Dermoptera		**0.047**	**0.010**	0.128	**0.039**	**0.039**
	Haplorrhini	**0.047**	-	0.088	**0.036**	0.765	0.850
	Lagomorpha	**0.010**	0.088	-	**0.001**	0.202	0.119
	Rodentia	0.128	**0.036**	**0.001**	-	**0.031**	**0.016**
	Scandentia	**0.039**	0.765	0.202	**0.031**	-	0.916
	Strepsirrhini	**0.039**	0.850	0.119	**0.016**	0.916	-

Table 6a. Results of phylogenetic analysis of variance (pANOVA) of residuals from PGLS regression of log_{10} petrosal lobule volume (mm^3) plotted against log_{10} adjusted endocranial volume (mm^3) (PLV~AEV) and log_{10} petrosal lobule mass (g) plotted against log_{10} adjusted body mass (g) (PLM~ABM) by primary ecological categories for locomotor behaviour, activity pattern, and diet in Euarchontoglires.

	Data		Df	SS	Residual SS	R^2	F	Z	sig. (*p*)
PLV~AEV	Locomotor Behaviour	Categories	8	0.030	0.004	0.101	1.843	1.221	0.117
		Residuals	131	0.267	0.002	0.899			
		Total	139	0.297					
	Activity Pattern	Categories	4	0.004	0.001	0.012	0.411	-0.653	0.772
		Residuals	135	0.293	0.002	0.988			
		Total	139	0.297					
	Diet	Categories	6	0.021	0.004	0.071	1.701	1.101	0.120
		Residuals	133	0.276	0.002	0.929			
		Total	139	0.297					
PLM~ABM	Locomotor Behaviour	Categories	8	0.088	0.011	0.200	4.106	2.539	**0.002**
		Residuals	131	0.349	0.003	0.800			
		Total	139	0.437					
	Activity Pattern	Categories	4	0.0047	0.001	0.011	0.367	-0.810	0.806
		Residuals	135	0.432	0.003	0.989			
		Total	139	0.437					
	Diet	Categories	6	0.031	0.005	0.070	1.677	1.074	0.146
		Residuals	130	0.406	0.003	0.930			
		Total	136	0.437					

Table 6b. Results of post hoc tests based on phylogenetic analysis of variance (pANOVA) of residuals from PGLS regression of log_{10} petrosal lobule mass (g) plotted against log_{10} adjusted body mass (g) (PLM~ABM) for locomotor behaviour in Euarchontoglires.

Order	Ar	Cu	Fo	Gl	Sl	Sc	Sa	SAr	Tr
Arboreal	-	0.762	**0.007**	0.38	0.973	0.051	0.712	0.681	0.719
Cursorial	0.762	-	0.074	0.422	0.607	0.301	0.982	0.965	0.85
Fossorial	**0.007**	0.074	-	0.269	0.069	0.097	**0.032**	**0.034**	**0.004**
Gliding	0.38	0.422	0.269	-	0.526	0.977	0.387	0.366	0.307
Saltatorial	0.973	0.607	0.069	0.526	-	0.367	0.741	0.759	0.828
Scansorial	0.051	0.301	0.097	0.977	0.367	-	0.215	0.184	**0.001**
Semiaquatic	0.712	0.982	**0.032**	0.387	0.741	0.215	-	0.975	0.815
Slow arboreal	0.681	0.965	**0.034**	0.366	0.759	0.184	0.975	-	0.857
Terrestrial	0.719	0.85	**0.004**	0.307	0.828	**0.001**	0.815	0.857	-

Arboreal (Ar), Cursorial (Cu), Fossorial (Fo.), Gliding (Gl), Saltatorial (Sl), Scansorial (Sc), Semiaquatic (Sa), Slow Arboreal (SAr) Terrestrial (Tr).

Table 7. Results of phylogenetic analysis of variance (pANOVA) of residuals from PGLS regression of log_{10} petrosal lobule volume (mm^3) plotted against log_{10} adjusted endocranial volume (mm^3) (PLV~AEV) and log_{10} petrosal lobule mass (g) plotted against log_{10} adjusted body mass (g) (PLM~ABM) by primary ecological categories for locomotor behaviour, activity pattern, and diet in Rodents.

	Data		Df	SS	Residual SS	R^2	F	Z	sig. (*p*)
PLV~AEV	Locomotor Behaviour	Categories	6	0.028	0.005	0.124	1.511	0.937	0.160
		Residuals	64	0.196	0.003	0.876			
		Total	70	0.224					
	Activity Pattern	Categories	4	0.004	0.001	0.017	0.292	-1.009	0.855
		Residuals	66	0.220	0.003	0.983			
		Total	70	0.224					
	Diet	Categories	4	0.024	0.005	0.106	1.544	0.896	0.176
		Residuals	33	0.200	0.003	0.894			
		Total	37	0.224					
PLM~ABM	Locomotor Behaviour	Categories	6	0.043	0.007	0.168	2.161	1.486	0.051
		Residuals	64	0.214	0.003	0.832			
		Total	70	0.258					
	Activity Pattern	Categories	4	0.003	0.001	0.014	0.227	-1.396	0.927
		Residuals	66	0.254	0.004	0.986			
		Total	70	0.258					
	Diet	Categories	4	0.029	0.006	0.111	1.631	0.973	0.152
		Residuals	33	0.229	0.004	0.889			
		Total	37	0.258					

Table 8. Results of phylogenetic analysis of variance (pANOVA) of residuals from PGLS regression of log_{10} petrosal lobule volume (mm^3) plotted against log_{10} adjusted endocranial volume (mm^3) (PLV~AEV) and log_{10} petrosal lobule mass (g) plotted against log_{10} adjusted body mass (g) (PLM~ABM) by primary ecological categories for locomotor behaviour, activity pattern, and diet in Primates.

	Data		Df	SS	Residual SS	R^2	F	Z	sig. (*p*)
PLV~AEV	Locomotor Behaviour	Categories	2	0.001	0.000	0.012	0.213	-0.672	0.784
		Residuals	35	0.192	0.003	0.880			
		Total	37	0.218					
	Activity Pattern	Categories	2	0.000	0.000	0.009	0.164	-0.950	0.849
		Residuals	35	0.043	0.001	0.991			
		Total	37	0.044					
	Diet	Categories	4	0.005	0.001	0.105	0.965	0.261	0.451
		Residuals	33	0.039	0.001	0.895			
		Total	37	0.044					
PLM~ABM	Locomotor Behaviour	Categories	2	0.000	0.000	0.006	0.109	-1.192	0.896
		Residuals	35	0.069	0.002	0.994			
		Total	37	0.069					
	Activity Pattern	Categories	2	0.001	0.000	0.009	0.151	-0.977	0.853
		Residuals	35	0.068	0.002	0.991			
		Total	37	0.069					
	Diet	Categories	4	0.008	0.002	0.119	1.113	0.441	0.349
		Residuals	33	0.061	0.002	0.881			
		Total	37	0.069					

Table 9a. Comparisons of evolutionary model fit for petrosal lobules volume based on residuals of OLS regression of log_{10} petrosal lobule volume (mm^3) plotted against log_{10} adjusted endocranial volume (mm^3).

Model	fit	ΔAICc	W_A
Euarchontoglires			
BM1	174.70	78.07	0.00
OU1	**96.63**	**0.00**	**0.48**
OUMloc	**98.56**	**1.94**	**0.18**
OUMact	98.67	2.05	0.17
OUMdiet	98.64	2.01	0.17
Rodentia			
BM1	**-20.20**	**1.58**	**0.17**
OU1	**-21.78**	**0.00**	**0.36**
OUMloc	**-20.51**	**1.26**	**0.19**
OUMact	**-20.11**	**1.66**	**0.16**
OUMdiet	-19.56	2.21	0.12
Primates			
BM1	54.57	5.58	0.03
OU1	**48.99**	**0.00**	**0.54**
OUMloc	51.95	2.96	0.12
OUMact	52.37	3.38	0.10
OUMdiet	51.01	2.02	0.20

Table 9b. Comparisons of evolutionary model fit for petrosal lobules volume based on residuals of OLS regression of and log_{10} petrosal lobule mass (g) plotted against log_{10} adjusted body mass (g).

Model	fit	ΔAICc	W_A
Euarchontoglires			
BM1	270.88	128.84	0.00
OU1	**142.04**	**0.00**	**0.95**
OUMloc	150.14	8.10	0.02
OUMact	150.12	8.08	0.02
OUMdiet	150.21	8.16	0.02
Rodentia			
BM1	63.24	2.84	0.12
OU1	**60.40**	**0.00**	**0.50**
OUMloc	62.77	2.37	0.15
OUMact	63.68	3.28	0.10
OUMdiet	62.99	2.60	0.14
Primates			
BM1	-3.99	5.85	0.03
OU1	**-9.32**	**0.51**	**0.38**
OUMloc	**-9.83**	**0.00**	**0.49**
OUMact	-4.45	5.39	0.03
OUMdiet	-5.72	4.11	0.06